

SUPPLEMENTARY MATERIAL

of

Global-scale environmental niche and habitat of blue shark (*Prionace glauca*) by size and sex: a pivotal step to improving stock management

Jean-Noël Druon¹, Steven Campana², Frederic Vandeperre^{3,4}, Fábio H.V. Hazin⁵, Heather Bowlby⁶, Rui Coelho^{7,8}, Nuno Queiroz^{9,10}, Fabrizio Serena¹¹, Francisco Abascal¹², Dimitrios Damalas¹³, Michael Musyl¹⁴, Jon Lopez¹⁵, Barbara Block¹⁶, Pedro Afonso^{3,4}, Heidi Dewar¹⁷, Philippe S. Sabarros^{18,19}, Brit Finucci²⁰, Antonella Zanzi¹, Pascal Bach^{18,19}, Inna Senina²¹, Fulvio Garibaldi²², David W. Sims^{23,24}, Joan Navarro²⁵, Pablo Cermeño²⁶, Agostino Leone^{18,27}, Guzmán Díez²⁸, María Teresa Carreón Zapiain²⁹, Michele Deflorio³⁰, Evgeny V. Romanov³¹, Armelle Jung³², Matthieu Lapinski³³, Malcolm Francis³⁴, Humberto Hazin³⁵, Paulo Travassos³⁶

¹ Joint Research Centre (JRC), European Commission, Ispra, Italy

² Life and Environmental Sciences, University of Iceland, Reykjavik, Iceland

³ Okeanos, University of the Azores, Horta, Portugal

⁴ IMAR - Institute of Marine Research, University of the Azores, Horta, Portugal

⁵ Universidade Federal Rural de Pernambuco, Recife, Pernambuco, Brazil

⁶ Fisheries and Oceans Canada, Bedford Institute of Oceanography, Dartmouth, Canada

- ⁷ IPMA - Portuguese Institute for the Ocean and Atmosphere, I.P. Olhão, Portugal
- ⁸ CCMAR - Center of Marine Sciences of the Algarve. Univ. Algarve, Faro, Portugal
- ⁹ CIBIO, Centro de Investigação em Biodiversidade e Recursos Genéticos, InBIO Laboratório Associado, Campus de Vairão, Universidade do Porto, 4485-661 Vairão, Portugal
- ¹⁰ BIOPOLIS Program in Genomics, Biodiversity and Land Planning, CIBIO, Campus de Vairão, 4485-661 Vairão, Portugal
- ¹¹ CNR IRBIM-National Research Council – Institute of Marine Biological Resources and Biotechnologies, Mazara del Vallo, Italy
- ¹² Spanish National Research Council. Spanish Institute of Oceanography, Santa Cruz de Tenerife, Spain
- ¹³ Hellenic Centre for Marine Research, Institute of Marine Biological Resources and Inland Waters, P.O. Box 2214, 71003 Heraklion, Greece
- ¹⁴ Pelagic Research Group LLC, P.O. Box 10243, Honolulu, HI 96816, USA
- ¹⁵ Inter-American Tropical Tuna Commission, Ecosystem and Bycatch Program, La Jolla, USA
- ¹⁶ Hopkins Marine Station, Stanford University, Monterey, CA, USA
- ¹⁷ National Oceanic and Atmospheric Administration (NOAA), Southwest Fisheries Science Center, Monterey, CA, USA
- ¹⁸ MARBEC, Univ Montpellier, CNRS, Ifremer, IRD, Sète, France
- ¹⁹ Institut de Recherche pour le Développement (IRD), Observatoire des Ecosystèmes Pélagiques Tropicaux Exploités (Ob7), Sète, France
- ²⁰ National Institute of Water and Atmospheric Research (NIWA), Wellington, New Zealand
- ²¹ MEMMS (Marine Ecosystems Modeling and Monitoring by Satellites), CLS, Space Oceanography Division, 8-10 rue Hermes, 31520 Ramonville, France
- ²² Department of Earth Sciences, Environmental and Life, University of Genova, Genova, Italy
- ²³ Marine Biological Association of the United Kingdom, The Laboratory, Citadel Hill, Plymouth, UK
- ²⁴ Ocean and Earth Science, National Oceanography Centre Southampton, University of Southampton, Southampton, UK
- ²⁵ Institut de Ciències el Mar (ICM-CSIC), Barcelona, Spain
- ²⁶ Research and in situ Conservation Department, Barcelona Zoo, Spain
- ²⁷ Department of Biological, Geological and Environmental Sciences, Laboratory of Genetics and Genomics of Marine Resources and Environment, University of Bologna, Ravenna, Italy

²⁸ AZTI, Marine Research, Basque Research and Technology Alliance (BRTA), Sukarrieta - Bizkaia, Spain

²⁹ Laboratorio de Ecología Pesquera, Unidad B. Facultad de Ciencias Biológicas, Universidad Autónoma de Nuevo León, Mexico

³⁰ Department of Veterinary Medicine, University of Bari Aldo Moro, Valenzano, Italy

³¹ CITEB - Centre technique de recherche et de valorisation des milieux aquatiques, Le Port, Île de La Réunion, France

³² Des Requins et Des Hommes (DRDH), Technopole Brest-Iroise, France

³³ Association AILERONS, Université Montpellier 2, Montpellier, France

³⁴ National Institute of Water and Atmospheric Research (NIWA), Wellington, New Zealand

³⁵ DCN- Department of Animal Science, Federal Rural University of Semiarid, Mossoró, Brazil

³⁶ Universidade Federal Rural de Pernambuco – UFRPE, Dept. de Pesca e Aquicultura, Recife, Brazil

Correspondence:

Jean-Noël Druon, Directorate D – Sustainable Resources, Joint Research Centre (JRC), European Commission, Ispra, Italy. Email: jean-noel.druon@ec.europa.eu

Table of contents

SUPPLEMENTARY MATERIAL

of

Global-scale environmental niche and habitat of blue shark (*Prionace glauca*) by size and sex: a pivotal step to improving stock management

Table of contents

Density maps by size and sex classes of presence data

Filtering criteria for the geolocation of electronic tagging data

Presence data used for the model calibration and validation

Chlorophyll-a gradient calculation

Mesopelagic micronekton predictions

Environmental and habitat data integration

Cluster analysis method and illustrative abiotic variables

Model performance and size of core habitat

Mesopelagic micronekton and SST distributions

The extreme abiotic conditions in the Northwest Atlantic Ocean

Further qualitative model validation with literature

Regional interannual mean and trends of foraging habitat

References

Density maps by size and sex classes of presence data

Below are the distribution maps of blue shark presence data used for the model calibration and validation by class of size and sex including fisheries observer data and the highest position accuracy data from electronic tags. See Table SM.1 for details on the number of data used for the calibration of each model parameter, as well as for the model validation.

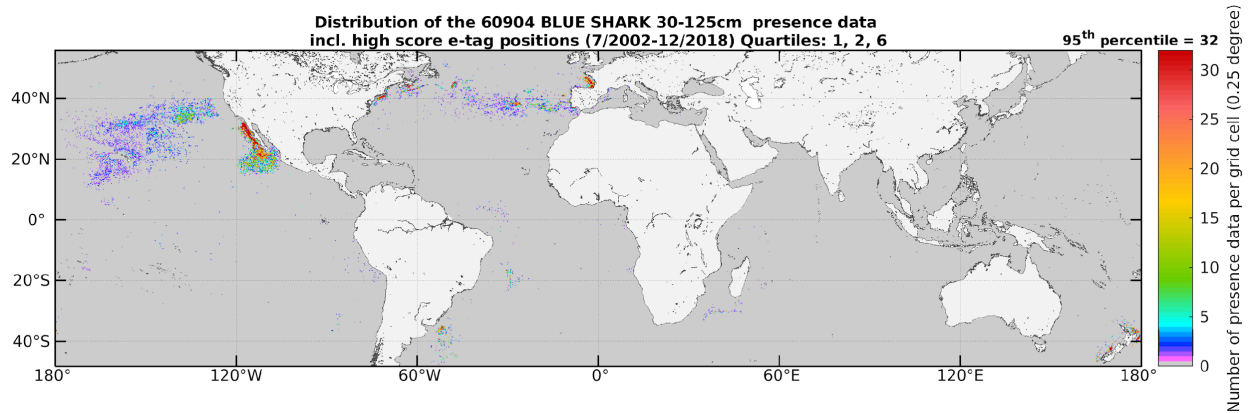


Figure SM.1 Distribution of both calibration and validation presence data of the small juvenile blue sharks (FL < 125 cm, n = 60,904, number of presence data per grid cell of 0.25°). These data include fisheries observer data and the highest position accuracy data from electronic tags.

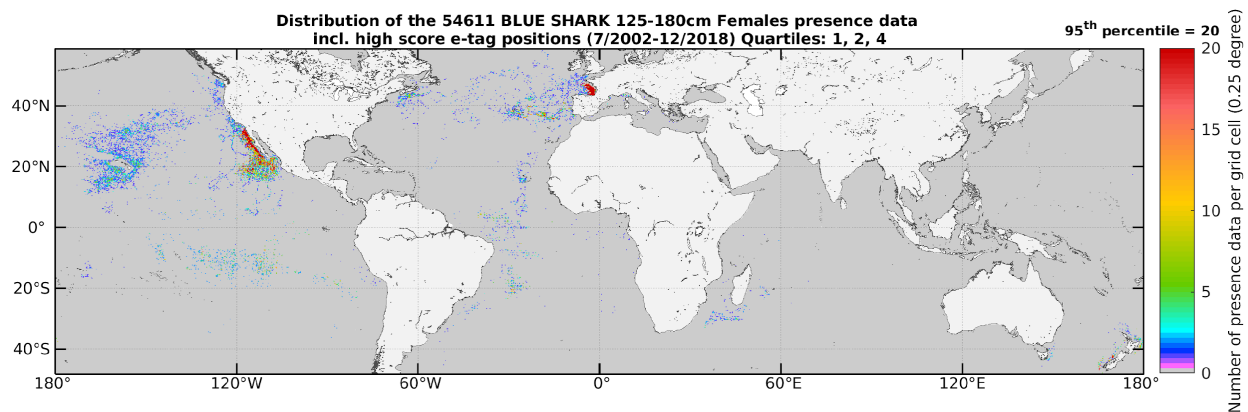


Figure SM.2 Distribution of both calibration and validation presence data of the large female blue sharks (125 cm < FL < 180 cm, n = 54,611, number of presence data per grid cell of 0.25°). These data include fisheries observer data and the highest position accuracy data from electronic tags.

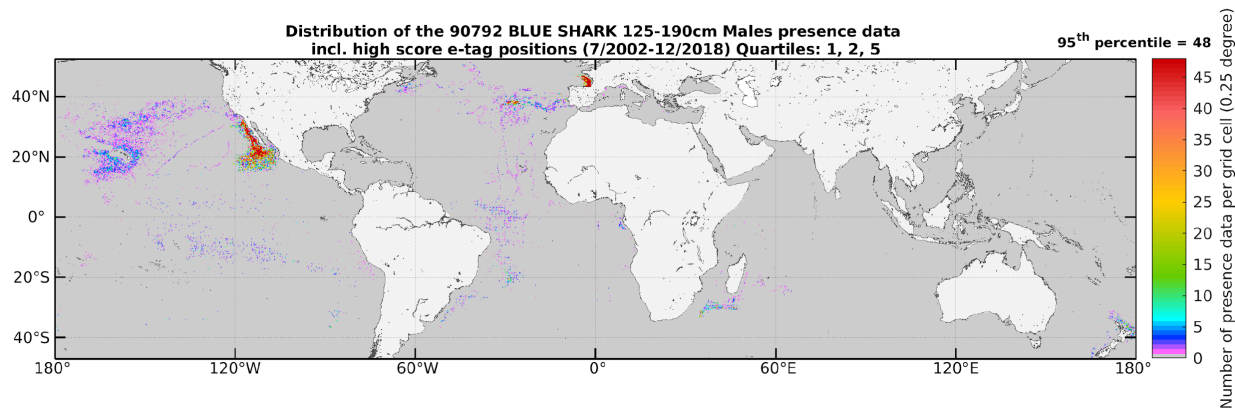


Figure SM.3 Distribution of both calibration and validation presence of the large male blue sharks (125 cm < FL < 190 cm, n = 90,792, number of presence data per grid cell of 0.25°). These data include fisheries observer data and the highest position accuracy data from electronic tags.

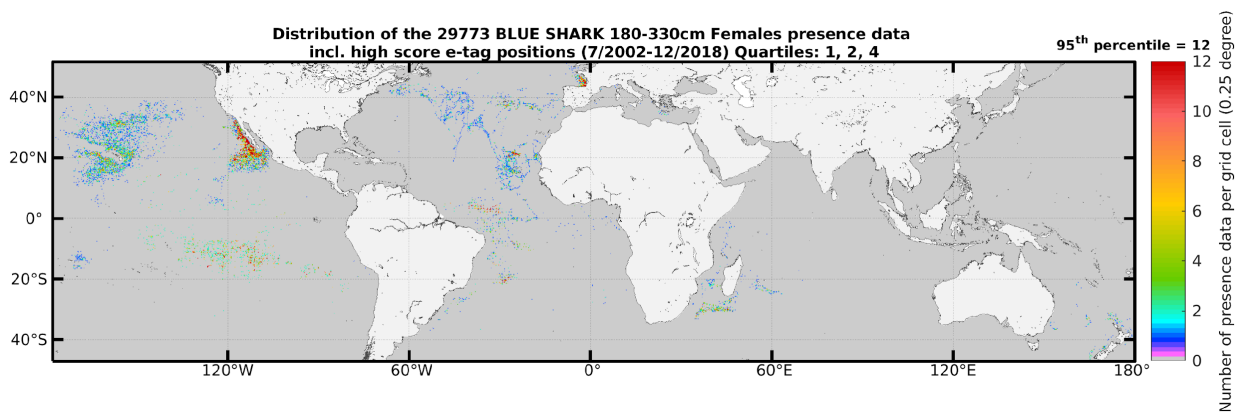


Figure SM.4 Distribution of both calibration and validation presence data of the adult female blue sharks (180 cm < FL < 330 cm, n = 29,773, number of presence data per grid cell of 0.25°). These data include observer fisheries data and the highest position accuracy data from electronic tags.

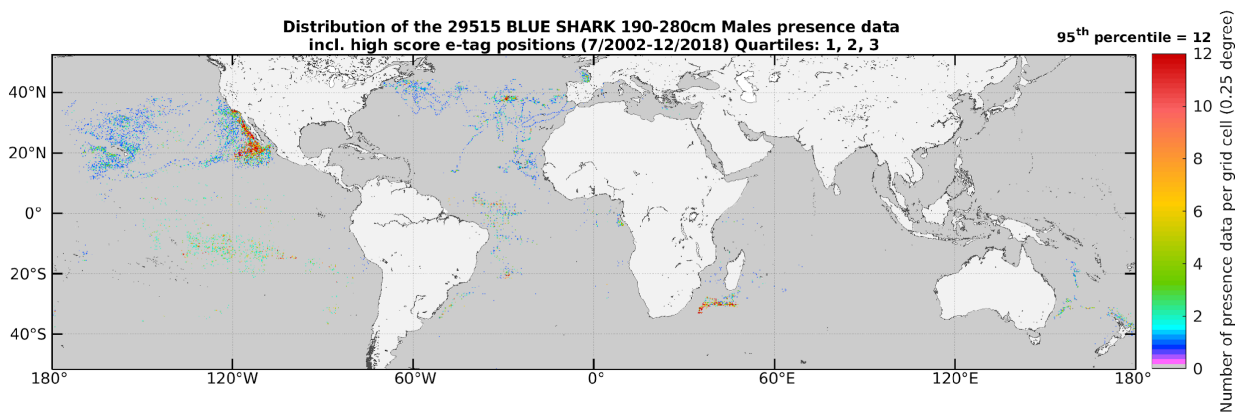


Figure SM.5 Distribution of both calibration and validation presence data of the large female blue sharks (190 cm < FL < 280 cm, n = 29,515, number of presence data per grid cell of 0.25°). These data include fisheries observer data and the highest position accuracy data from electronic tags.

Filtering criteria for the geolocation of electronic tagging data

A total of 234 tracks from electronically tagged blue sharks in the Pacific (95), Atlantic (132), and Indian Oceans (7) using different types of electronic tags (SPOT, PSAT, and miniPAT tags) were included in the environmental analysis (see also the seven habitat animations with the overlay of electronic tagging and observer data as separate SM). These data were filtered in terms of positioning quality following various criteria. To ensure short-term movements were realistic, we first filtered out tag positions that would have required the animal to exceed a daily mean velocity of 8 knots when moving between two consecutive positions (Queiroz et al. 2016). We then only kept the best quality positions. For SPOT and PTT tags, we rejected the points with no accuracy estimation and we kept location classes above or equal to 0 (higher precision than 5 km, Costa et al. 2010). For PSAT and miniPAT tags, position estimates were derived from an integrated state-space hidden Markov model called GPE3 (Wildlife Computers; Pedersen et al. 2011). We retained points if the observation score was above 50 (on a 0-100 scale), indicating a close match between the location suggested by the observation and the modeled location. Finally, we selected the first high-precision location from each day to limit oversampling in the same environment and reduce serial autocorrelation. As is typical when multiple data types are combined, there were differences in the resolution of the position estimates.

Presence data used for the model calibration and validation

The criterion for selecting the calibration data was a minimum *CHL* coverage (5-day integrated) of 35% in a 25 km radius centered on the presence data, following its location precision (about 50 km) to extract suitable environmental data. If it did not meet this calibration criterion, validation data needed to meet a minimum level of habitat coverage (5-day integrated). The functional form of minimum habitat coverage of the validation data decreased with an increasing distance to the pixel of the presence data following:

$$\text{Minimum coverage of 5-day habitat centered on presence data (\%)} = (np + 0.5)^{-0.4}$$

with np , the window size in pixels centered on the presence data (e.g., values of np of 1 [9 central cells], 5 [81 central cells], and 10 [441 central cells] correspond to a minimum coverage of 85%, 51%, and 39%, respectively). This decreasing criterion of habitat coverage farther from the data location was thus used

to accept the validation data, and was furthermore needed to compute relevant distances of presence data to the closest suitable habitat.

The number of presence data by size and sex class used for the model calibration is different due to variable i) coverage of environmental data (e.g., *CHL*), and ii) used distributions (cluster analysis or global, below or above CHL_{min} for biotic proxies). Table SM.1 summarizes the number of presence data used for the calibration of each class and type of environmental variable. The number of independent presence data used for the validation that depends on the habitat coverage around each presence data is also indicated.

Table SM.1 Number of presence data by size and sex class that were used for the calibration (mean environmental value in a 25 km-radius centered on the presence data) and validation of the blue shark foraging habitat model (07/2002-12/2018). *SJ*: small juvenile blue sharks; *LJF*: large juvenile females; *LJM*: large juvenile males; *AF*: adult females; *AM*: adult males; *gradCHL_{int}**: global distribution of 5-day mean horizontal gradient of sea surface chlorophyll-a (number of presence data only for $CHL_{min} < CHL < CHL_{max}$) (see Figure 3); *MMnekt_{int}***: global distribution of mesopelagic micronekton (number of presence data only for $CHL < CHL_{min}$) (see Figure 3); *Abiotic – SST, SSHa (SST_{min/max}, SSHa_{min/max})****: global distributions of abiotic variables (see Figure 4); *Clustering – biotic & abiotic (CHL_{min/max}, gradCHL_{min}, MMnekt_{int}, SST_{intermediate avoidance})*****: cluster analysis using simultaneous availability of biotic and abiotic variables (see Figure 4 and Figures SM.7-11).

Number of presence data	Available	Calibration (% of available)	Validation (% of available)
<i>SJ</i>	60,904 (23%)	<i>Biotic – gradCHL_{int}*</i> 11,918 (20%)	25,563 (42%)
		<i>Biotic - MMnekt_{int}**</i> 3,368 (6%)	
		<i>Abiotic – SST, SSHa***</i> 27,343 (45%)	
		<i>Clustering – biotic & abiotic****</i> 13,334 (22%)	
<i>LJF</i>	54,611 (21%)	<i>Biotic – gradCHL_{int}</i> 11,416 (21%)	26,366 (48%)
		<i>Biotic - MMnekt_{int}</i> 4,948 (9%)	
		<i>Abiotic – SST, SSHa</i> 27,761 (51%)	
		<i>Clustering – biotic & abiotic</i> 14,665 (27%)	
		<i>Biotic – gradCHL_{int}</i> 13,902 (15%)	

<i>LJM</i>	90,792 (34%)	<i>Biotic - MMnekton_{int}</i> 6,763 (7%)	44,298 (49%)
		<i>Abiotic – SST, SSHa</i> 33,640 (37%)	
		<i>Clustering – biotic & abiotic</i> 18,815 (21%)	
<i>AF</i>	29,773 (11%)	<i>Biotic – gradCHL_{int}</i> 2,057 (7%)	15,594 (52%)
		<i>Biotic - MMnekton_{int}</i> 5,847 (20%)	
		<i>Abiotic – SST, SSHa</i> 13,552 (46%)	
		<i>Clustering – biotic & abiotic</i> 7,054 (24%)	
<i>AM</i>	29,515 (11%)	<i>Biotic – gradCHL_{int}</i> 3,044 (10%)	14,004 (47%)
		<i>Biotic - MMnekton_{int}</i> 5,260 (18%)	
		<i>Abiotic – SST, SSHa</i> 13,158 (45%)	
		<i>Clustering – biotic & abiotic</i> 7,833 (27%)	
<i>Total</i>	265,595 (100%)	<i>Biotic – gradCHL_{int}</i> 42,337 (16%)	125,825 (47%)
		<i>Biotic - MMnekton_{int}</i> 26,186 (10%)	
		<i>Abiotic – SST, SSHa</i> 115,454 (43%)	
		<i>Clustering – biotic & abiotic</i> 61,701 (23%)	

Chlorophyll-a gradient calculation

The daily chlorophyll-a data were pre-processed using iterations of a median filter to recover missing values on the edge of the valid data, followed by a Gaussian smoothing procedure to remove eventual sensor stripes (Druon et al. 2012; 2021). The norm of the chlorophyll-a gradient (*gradCHL*) was derived from the daily chlorophyll-a data, using a bi-directional gradient over a three-by-three grid-cell window as follows:

$$gradCHL = \sqrt{Gx^2 + Gy^2}$$

with Gx , Gy , the longitudinal and latitudinal chlorophyll-a horizontal gradient, respectively, corrected by the pixel size in km. Small and large chlorophyll-a fronts refer to variable levels of chlorophyll-a gradient values. The $gradCHL$ values, which are linked to the presence of pelagic species, were used in log-form to derive a dependent linear function at the basis of the daily foraging habitat in the mesotrophic environment (see Figure 3 of the main manuscript).

Mesopelagic micronekton predictions

Estimates of the mesopelagic micronekton distribution were extracted from the SEAPODYM-LTML (SEAPODYM for Low and Mid-Trophic Level organisms) model (Lehodey et al. 2015). SEAPODYM-LTML uses ocean currents, temperature, and primary production to simulate the dynamics of six functional groups of micronekton density representing the mid-trophic level organisms in the oceanic food web. Each functional group of micronekton occupies one or two pelagic layers depending on their diel vertical behavior. Both, upper mesopelagic and migrant upper mesopelagic groups occupy the upper mesopelagic layer (depth layer from 1.5 to 4.5-fold the euphotic depth) during the daytime, while organisms from the migrant group move up to the epipelagic layer (from 0 to 1.5-fold the euphotic depth) at night. The vertically-integrated primary production serves as a foraging proxy for the food web. The water temperature also controls the growth dynamics of the micronekton together with the new phytoplankton biomass (derived from primary production). The energy transferred from primary production to each functional group through the time-trophic continuum is calibrated from available data (Lehodey et al. 2015; Lehodey, Murtugudde, and Senina 2010). At each time step of micronekton production, the ocean currents averaged through the day and night in the pelagic layers are passively transporting micronekton biomass through the oceanic environment.

Environmental and habitat data integration

Figure SM.6 presents the overall integration of data from the original environmental to the habitat data. The daily interpolation from the monthly Copernicus environmental data from $1/12^\circ$ to $1/24^\circ$ resolution to the day of the blue shark observation was done to match the CHL and habitat grid and to provide the main seasonal variability. This integration over time, together within a 25-km radius, likely removed non-significant high variability from the daily data for this highly mobile large predator.

Original environmental data 2003-2018

- CHL (daily, $1/24^\circ$) – MODIS-Aqua sensor, NASA
- Upper mesopelagic micronekton (weekly, $1/12^\circ$) – SEAPODYM-LMTL, CMEMS
- SST, $T_{MLD+100}$, SSHa (monthly, $1/12^\circ$) – Global model *GLOBAL_REANALYSIS_PHY_001_030*, CMEMS



Interpolated environmental data 2003-2018 to the habitat grid (daily, $1/24^\circ$)

- CHL, gradCHL (daily, $1/24^\circ$)
- Upper mesopelagic micronekton (daily, $1/24^\circ$)
- SST, $T_{MLD+100}$, SSHa (daily, $1/24^\circ$)



Environmental data extraction at location of blue shark presence data for model calibration

- CHL, gradCHL (5-day centered on day of observation, 25 km radius mean)
- Upper mesopelagic micronekton (daily, 25 km radius mean)
- SST, $T_{MLD+100}$, SSHa (daily, 25 km radius mean)



Environmental data use for blue shark habitat (daily, $1/24^\circ$)

- CHL, gradCHL (daily, $1/24^\circ$)
- Upper mesopelagic micronekton (daily, $1/24^\circ$)
- SST, $T_{MLD+100}$, SSHa (daily, $1/24^\circ$)



Integrated blue shark habitat (seasonal 2003-2018, $1/24^\circ$) – Figures 5-9

- Step 1: daily to monthly habitat,
- Step 2: monthly to seasonal habitat 2003-2018.

Figure SM.6 Diagram summarizing the environmental data integration (time and resolution) to the habitat model grid spatial and temporal resolutions (daily, $1/24^\circ$), the integration for the environmental data extraction, and the integration from daily to seasonal 2003-2018 habitat.

Cluster analysis method and illustrative abiotic variables

Cluster analysis is a suitable method for identifying homogeneous groups of objects or ‘clusters’ (here, blue shark habitat suitability), regardless of their respective number. Cluster analysis is well suited to identify habitats that are marginally represented and may otherwise be interpreted as outliers by other statistical methods. The number of clusters was chosen as the minimum number that best separates distinct environments and favors interpretation (two or three clusters, see below). We used 5-day mean values of *CHL* and *gradCHL* to increase the number of matchups assuming that variability is low at ± 2 days from the sampling date and with the spatial resolution of $1/24^\circ$. *CHL* and *gradCHL* datasets were log-

transformed before use, due to the wide variability in their values, and were normalized by the mean and standard deviation before performing the cluster analysis.

K-means clustering (MacQueen 1967) based on a Euclidean distance was used to estimate the association of data points between clusters and to minimize the within-cluster sum of squared errors. In k-means clustering, the number of clusters k was first chosen (here the minimum number that favors interpretation) and the cluster centers were initialized randomly. Each data point was then assigned to the closest cluster based on a selected distance measure (similarity) and an updated cluster center. At each iteration step, the new cluster centers were computed as the mean vectors of the assigned data points. These two steps, data point assignment and cluster center update, were repeated until the cluster centers did not change anymore or until a sufficient number of iterations were performed. Matlab's k-means function was used with 500 iterations/restarts and the Euclidean distance setting. The z-score transformation (Berthold, Borgelt, and Höppner 2010) was performed before clustering, in which each data variable was normalized to zero mean and unit variance to guarantee that each selected variable had an equal influence on the minimization of the within-cluster sum of squares objective function (Berthold, Borgelt, and Höppner 2010).

The cluster analysis (Figures 4 and SM.7-11) was applied with non-influential (illustrative) variables to reveal the coherence of the results on blue shark habitat suitability concerning the abiotic conditions. The illustrative variables that were not included in the habitat model as displaying large variabilities were the sea surface salinity, sea surface current intensity, surface oxygen content, and the depth of the mixed layer. These variables were not identified as primary discriminant variables by the expert knowledge. The cumulative distribution of variables used in the clustering (black x-labels in Figure SM.7-11) highlights that the lowest chlorophyll-a level cluster ($CHL < CHL_{min}$), corresponding to the oligotrophic foraging of blue-shark, occurs in waters characterized by higher levels of temperature (SST and $T_{mid+100}$) and $SSH\alpha$, lower mesopelagic micronekton levels and deeper mesopelagic layer compared with the other clusters. These traits indeed characterize relatively poorly productive areas.

We choose a different number of clusters (three for the juveniles and two for the adults) to obtain consistent values of CHL_{min} between classes (0.09 to 0.13 mg.m⁻³). This selection also led to consistent results of the avoided intermediate range of SST by females with literature (see manuscript section "Consistency of model results with known traits and habitats"). When the selected number of clusters was two (i.e., for the adult blue sharks), the higher chlorophyll-a (and chlorophyll-a gradient) level cluster ($CHL_{min} < CHL < CHL_{max}$) on the contrary occurs for lower temperature and $SSH\alpha$ levels and higher

micronekton in a shallower mesopelagic layer, all characterizing relatively productive waters. When three clusters were retained (small and large juveniles), the third cluster showed intermediate levels for these variables, thus enhancing intermediate productivity levels, although occurring in relatively low SST levels, similar to the most productive waters. These intermediate productivity levels are to be related to particularly deep mixed layer depths in intermediate latitudes (about 30-40°).

Data for the abiotic variables (i.e. SST (° C), $T_{mld+100}$ (° C), SSHa (m), mixed layer depth (m), sea surface currents ($m \cdot s^{-1}$), sea surface salinity (psu), and sea surface oxygen ($mmol \cdot m^{-3}$), see Figures SM.7-11) are extracted from the EU-Copernicus Marine Environment Monitoring Service global model (<https://marine.copernicus.eu/access-data>). Monthly mean data are extracted from the global model (GLORYS12V1) with a $1/12^\circ$ horizontal resolution and 50 unevenly spaced vertical levels. These monthly data are interpolated onto the MODIS-Aqua grid ($1/24^\circ$ resolution) and then linearly interpolated to obtain daily values that match the sampling day. This month-to-day interpolation step is assumed to produce suitable estimates of the seasonal changes that define habitat. Surface values for temperature and salinity and current intensity are calculated from the upper model layer (ca. 4 m) while surface oxygen is the mean value over the upper 30 m. The mixed layer depth is defined as the maximum of the vertical density gradient.

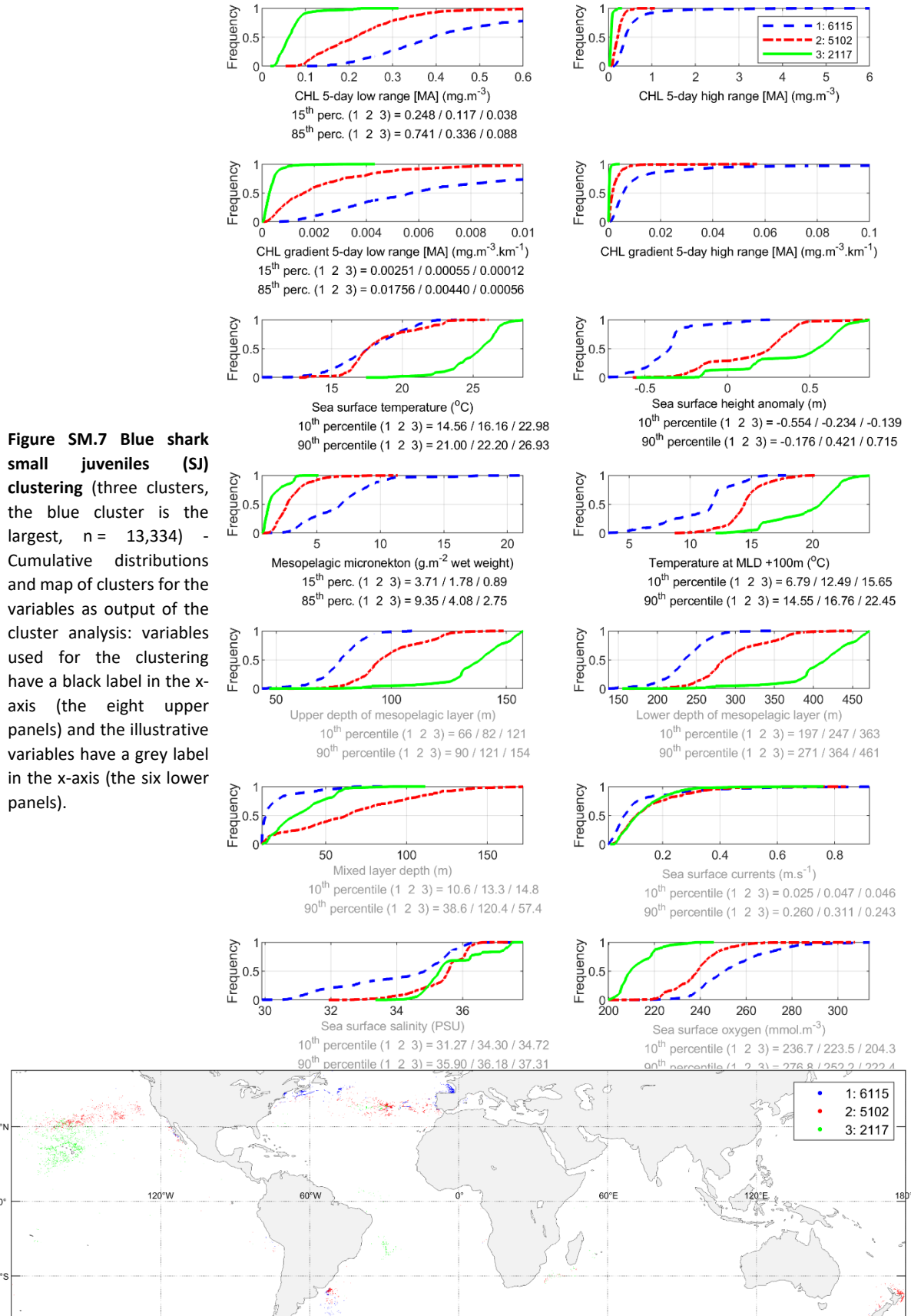


Figure SM.8 Blue shark large juvenile females (LJF) clustering (three clusters, the blue cluster is the largest, $n = 14,665$) - Cumulative distributions and map of clusters for the variables as output of the cluster analysis: variables used for the clustering have a black label in the x-axis (the eight upper panels) and the illustrative variables have a grey label in the x-axis (the six lower panels).

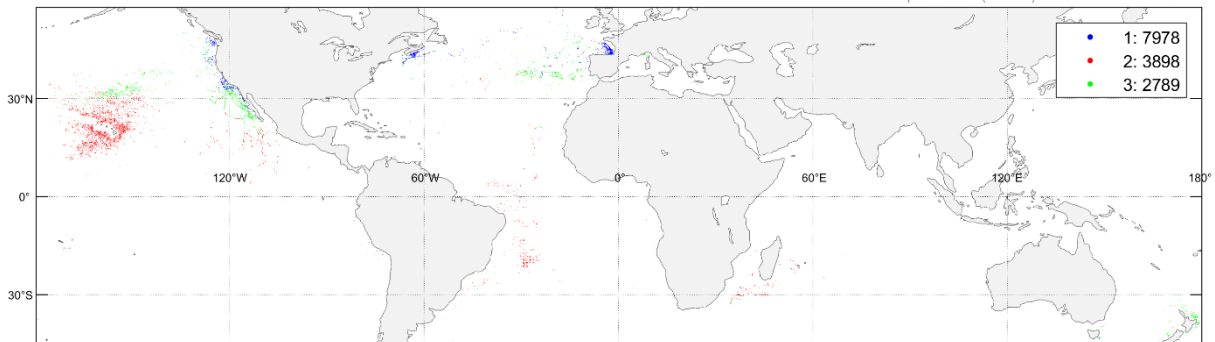
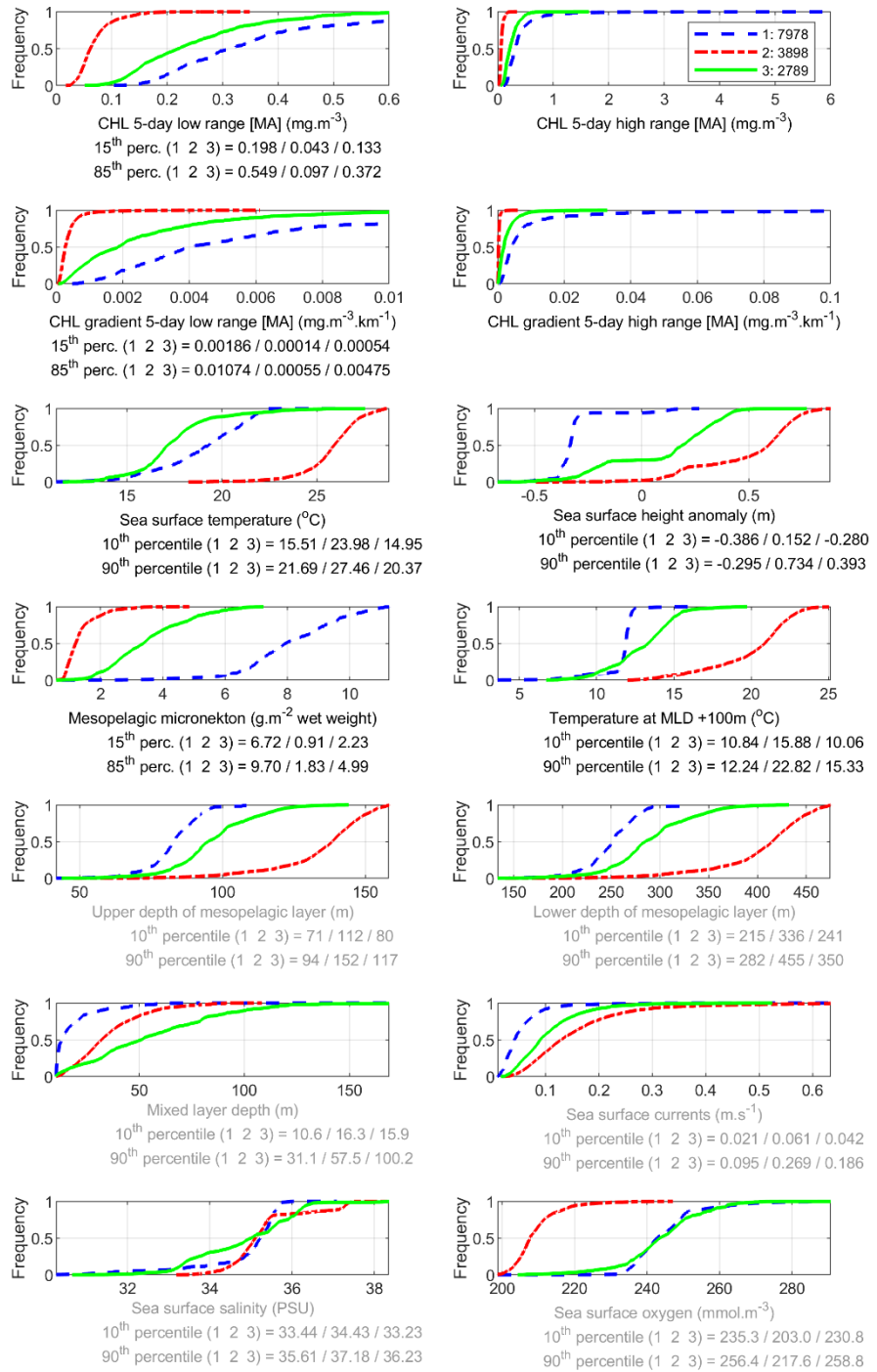


Figure SM.9 Blue shark large juveniles males (LJM) clustering (three clusters, the blue cluster is the largest, $n = 18,815$) - Cumulative distributions and map of clusters for the variables as output of the cluster analysis: variables used for the clustering have a black label in the x-axis (the eight upper panels) and the illustrative variables have a grey label in the x-axis (the six lower panels).

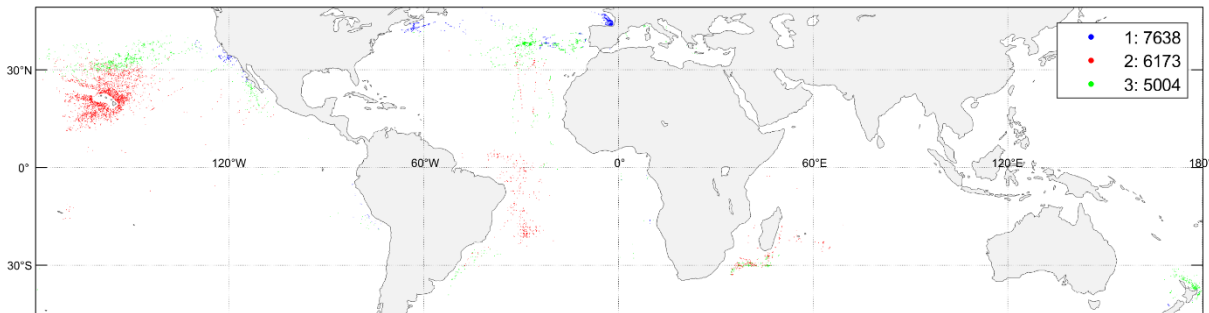
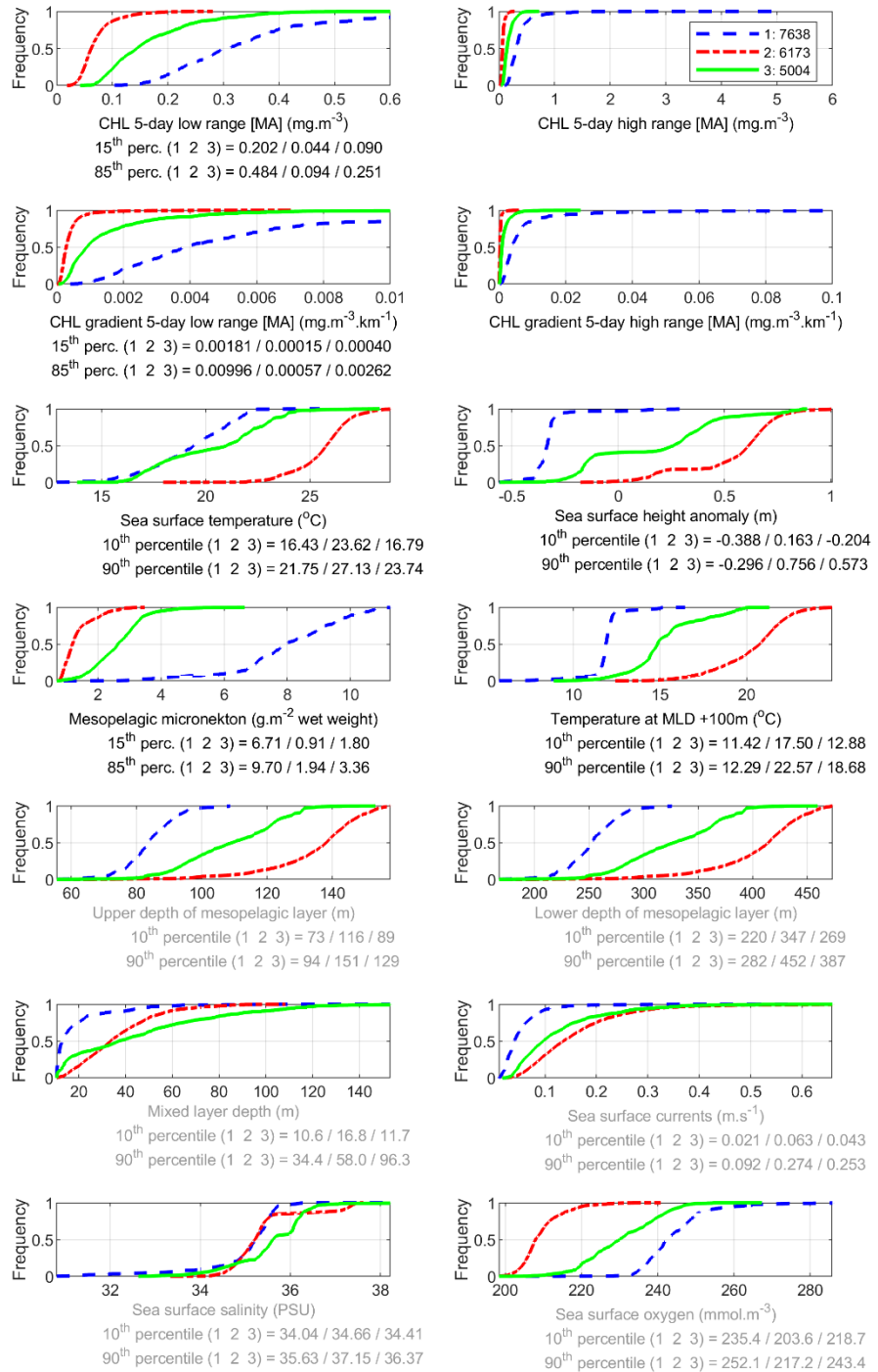


Figure SM.10 Blue shark adult females (AF) clustering (two clusters, the blue cluster is the largest, $n = 7,054$) - Cumulative distributions and map of clusters for the variables as output of the cluster analysis: variables used for the clustering have a black label in the x-axis (the eight upper panels) and the illustrative variables have a grey label in the x-axis (the six lower panels).

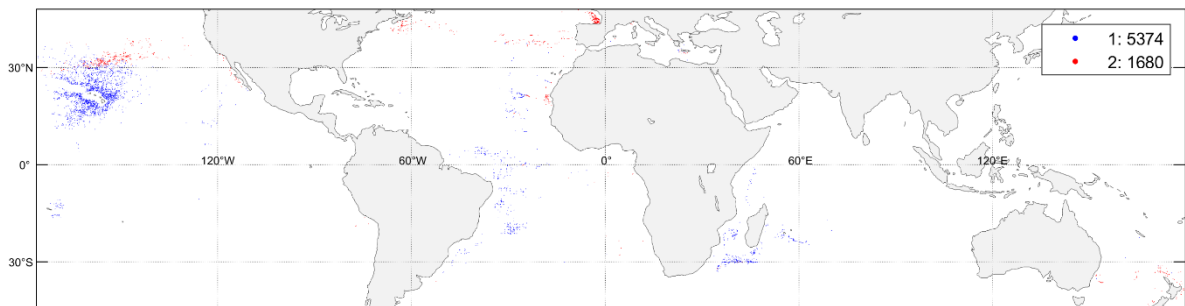
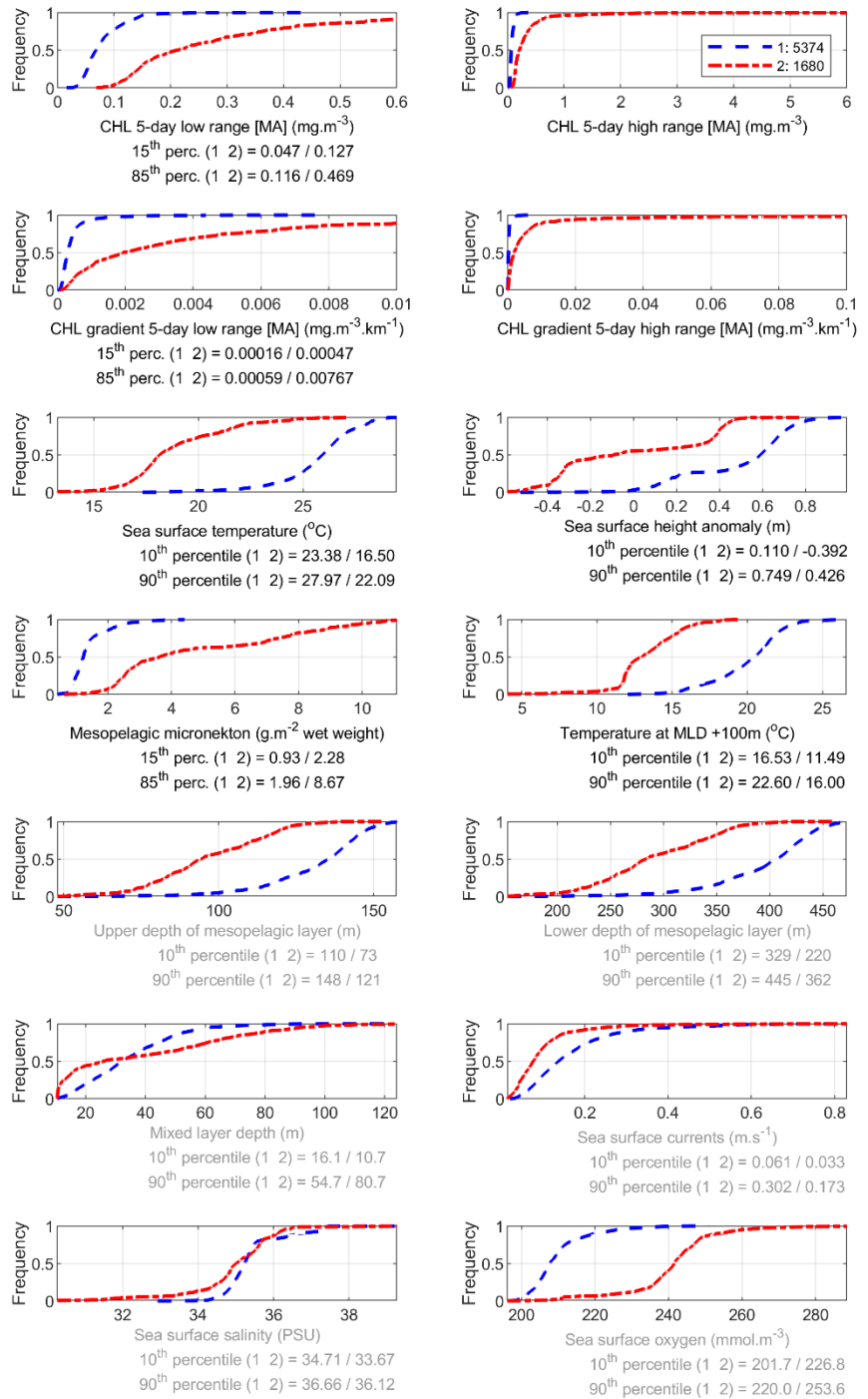
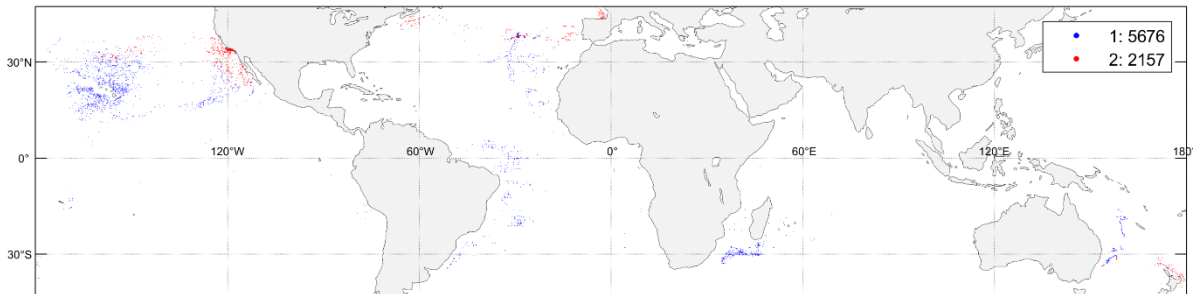
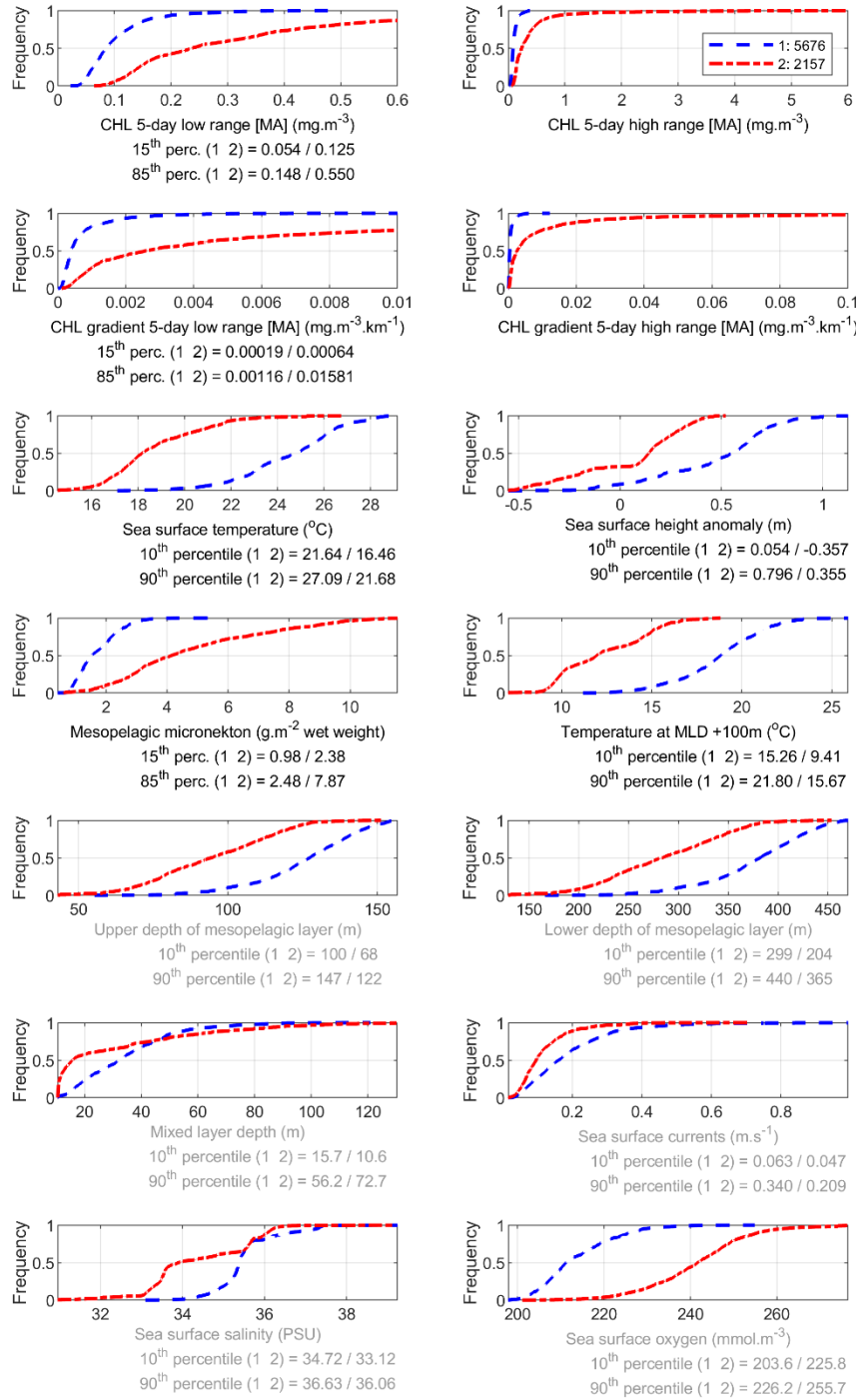


Figure SM.11 Blue shark adult males (AM) clustering (two clusters, the blue cluster is the largest, n = 7,833) - Cumulative distributions and map of clusters for the variables as output of the cluster analysis: variables used for the clustering have a black label in the x-axis (the eight upper panels) and the illustrative variables have a grey label in the x-axis (the six lower panels).



Model performance and size of core habitat

The main paper details the distribution of the distance of validation presence data to the closest core habitat boundary (km, above 30% favorable habitat, negative distances correspond to observation within the core habitat). We further detail that result in decomposing these distances by month and overlapping the corresponding mean habitat size (relative to the global ocean, %) to seasonally evaluate the model performance regarding the habitat surface area.

The model performance by month (Figure SM.12) displays relatively constant levels. The relative surface of the core habitat for each hemisphere (Figure SM.12) displays substantial seasonal variability as a larger poleward extent occurs during the warm months alternately in both hemispheres. A higher vulnerability to fishing may thus occur during the cold months alternatively in both hemispheres (generally November-May and May-September in the north and south hemispheres, respectively) following the likely contraction of the blue shark populations. Due to the tolerance to lower SSTs and larger range of SST avoidance, the LJF-class core habitat is more synchronous in both hemispheres with minima in November-December and April-June in the north hemisphere and in April-July in the south hemisphere. The range of the relative monthly surface area of the core habitat is about 18-22% \pm 2% and 23-29% \pm 2% in the north and south hemispheres, respectively, with larger and lower extents for SJ and AM, respectively. The habitat model is therefore relatively discriminant considering the large distribution of the species and model performance (86-99% of validation data closer than 50 km of the core habitat, see the main manuscript).

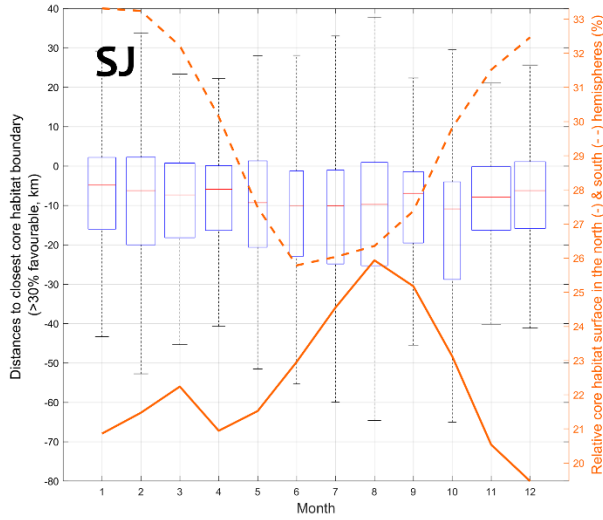
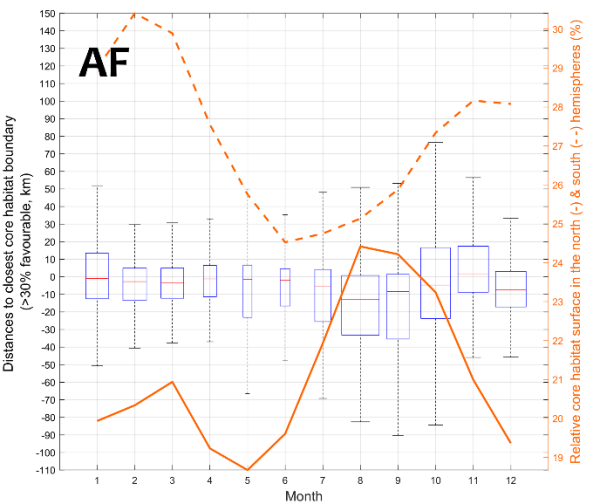
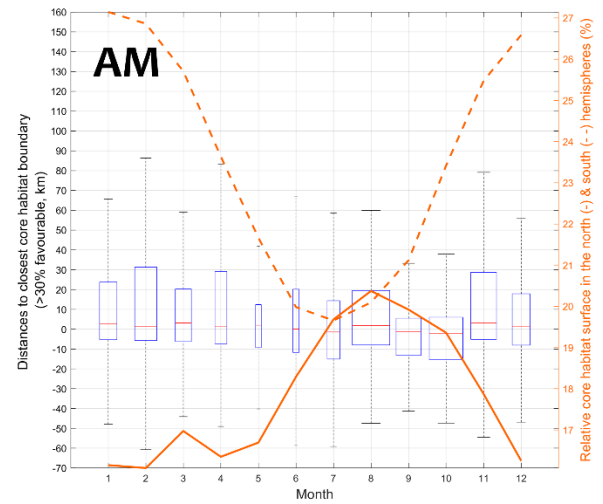
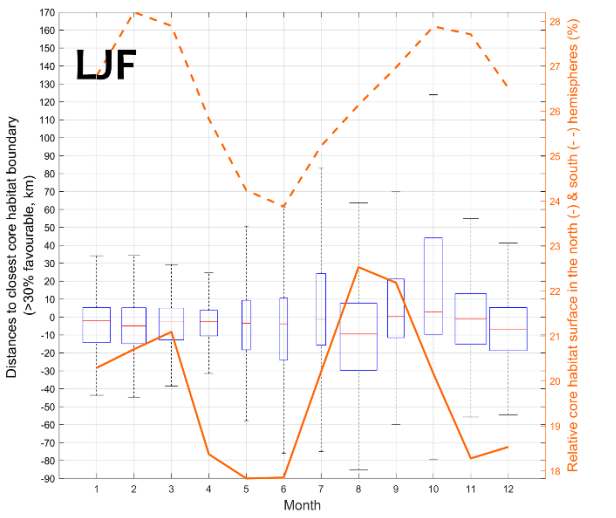
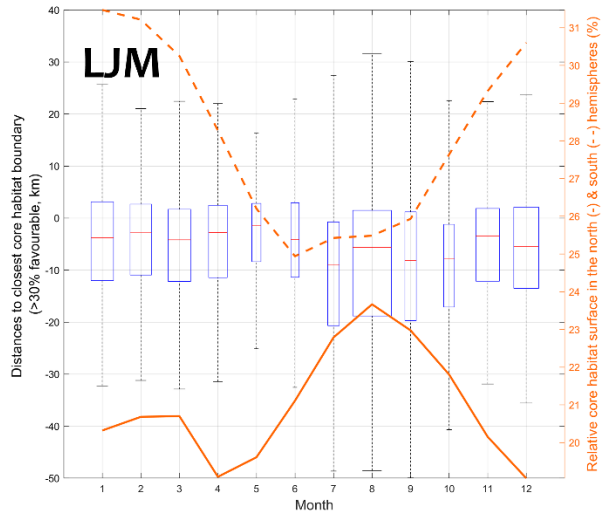


Figure SM.12 Details of model performance and relative habitat surface: monthly distribution of distance of validation presence data to closest core habitat boundary (km, above 30% favorable habitat, negative distances correspond to observation within the core habitat) and corresponding mean habitat surface (relative to the north (-) and south (-) hemispheres, %). The box width is proportional to the number of presence data, median values are indicated in red, and box limits are the 25th and 75th percentiles of the sample data. The value for whisker corresponds to approximately $\pm 2.7\sigma$ and 99.3 percent coverage if the data are normally distributed.



Mesopelagic micronekton and SST distributions

Below are the distribution maps of the upper mesopelagic micronekton (2003-2018) and SST (April-September and October-March 2003-2018) that highlight major unfavorable areas or differences of suitable habitat between classes (see legends for interpretation).

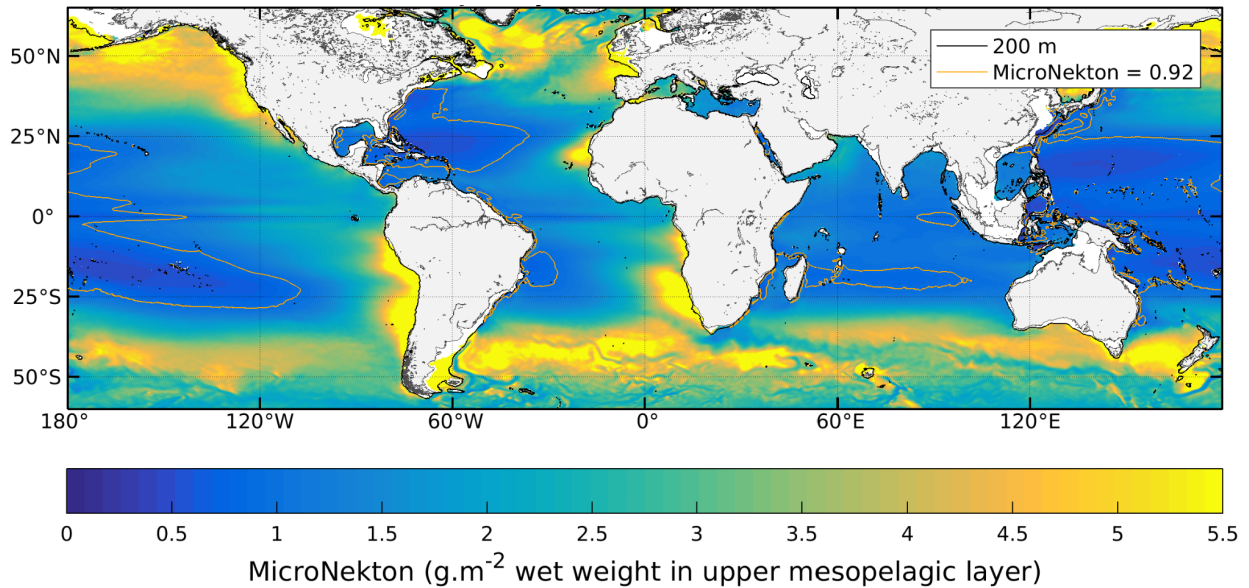


Figure SM.13 Distribution of mean mesopelagic micronekton (*MMneKton*, EU-Copernicus CMEMS) for the period 2003-2018. The isocontour of $0.92 \text{ g}\cdot\text{m}^{-2}$ wet weight (red lines) highlights the mean between blue shark classes of the minimum mesopelagic micronekton (*MMneKton_{min}*) limiting the foraging habitat suitability in most of the Western Central Pacific, in the tropical South-East Pacific west of 110°W , in the Sargasso Sea area, off Brazil between 12°S and 24°S and in the Indian Ocean mostly between 17°S and 24°S .

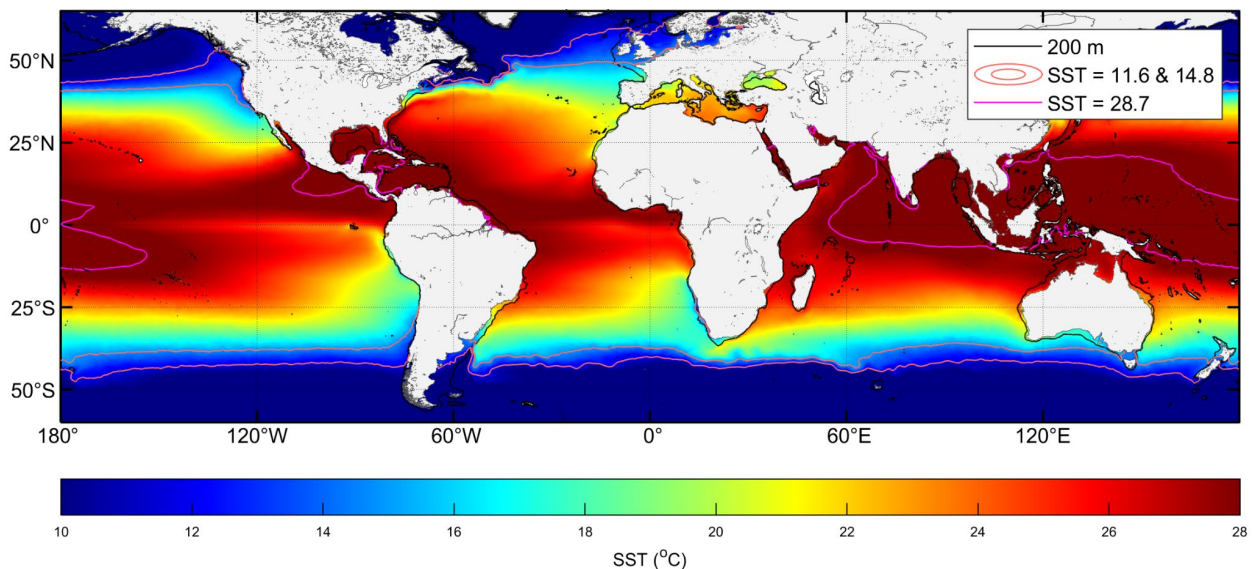


Figure SM.14 Distribution of mean sea surface temperature (SST, 0-5 m, EU-Copernicus CMEMS - GLORYS12V1) from **April to September** 2003-2018. SST isocontours of 11.6°C and 14.8°C (red lines) highlight the highest SST_{min} difference between the blue shark classes (large juvenile females – LJF and adult males – AM, respectively) and subsequent latitudinal differences of habitat during the warmest months in the northern hemisphere, and coldest months in the southern hemisphere. The SST isocontour of 28.7°C (pink line) is the mean SST_{max} level between classes reflecting the absence of favorable habitat in most of the Northeastern Indian Ocean and the Western Central Pacific Ocean (28.7°C is the mean upper SST limitation between all classes, $28.7^{\circ}\text{C} \pm 0.38$).

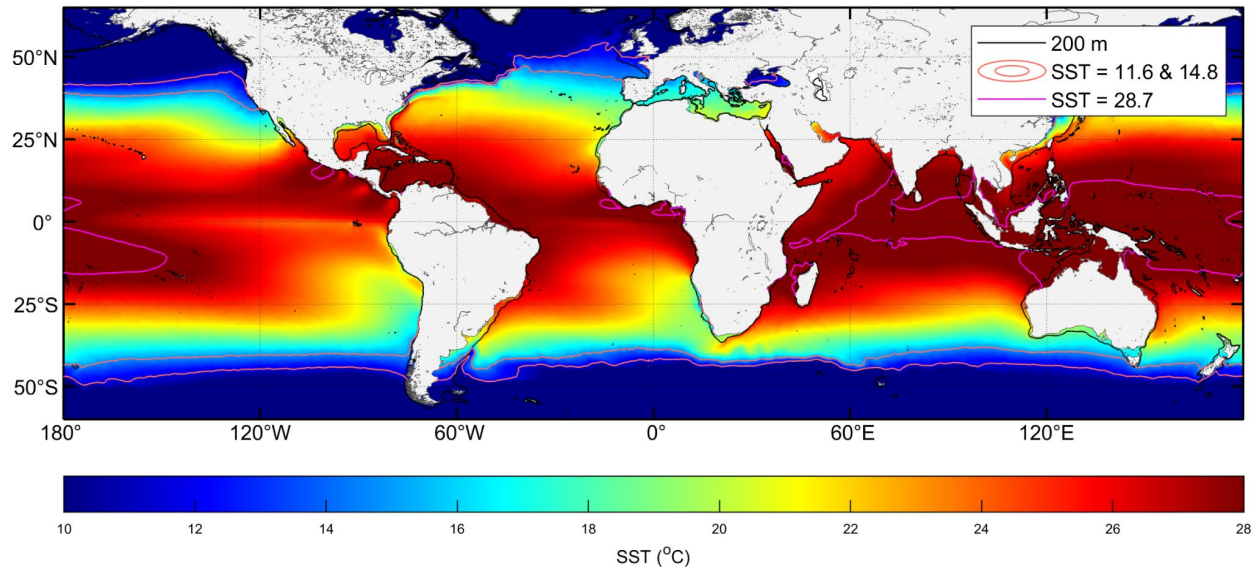


Figure SM.15 Distribution of mean sea surface temperature (SST, 0-5 m, EU-Copernicus CMEMS - GLORYS12V1) from **October to March** 2003-2018. SST isocontours of 11.6°C and 14.8°C (red lines) highlight the highest SST_{min} difference between the blue shark classes (large juvenile females – LJF and adult males – AM, respectively) and subsequent latitudinal differences of habitat during the coldest months in the northern hemisphere and warmest months in the southern hemisphere. The SST isocontour of 28.7°C (pink line) is the mean SST_{max} level between classes reflecting the absence of favorable habitat in most of the Central-eastern Indian Ocean and in the equatorial and tropical of the South-West Pacific Ocean (28.7°C is the mean upper SST limitation between all classes, $28.7^{\circ}\text{C} \pm 0.38$).

The extreme abiotic conditions in the Northwest Atlantic Ocean

We describe in the Methods section a particular situation in the Northwest Atlantic during winter where blue sharks were observed in the Nova Scotia shelf in winter (Campana et al. 2006) with SST levels below the tolerance temperature for all classes, as set in the model (below 11°C), but for which the temperature 100 m below the mixed layer depth ($T_{mld+100}$) is warmer and suitable for the SJ and LJF classes (above about 12°C) (Figure SM.16). We, therefore, included the specific situation in the modeling where suitable abiotic habitat is allowed when SST is lower than $T_{mld+100}$ and $T_{mld+100} > T_{mld+100 min}$. Noting that the same minimum criterion was taken for selecting SST_{min} and $SSHa_{min}$ (0.3th percentile value), Figure SM.16 (lower panel) also presents the corresponding suitable $SSHa$ levels for the SJ and LJF classes. These modeling results

agree with the minimum surface temperature of tagged blue sharks in this area (about 12-13°C in November) using electronic tagging [13 out of 23 tagged sharks were LJF, 6 were LJM] (Campana et al. 2011).

A maximum frequency of dive for adult males in the range of 100-230 m (depths of TMLD+100m) with a minimum temperature of about 15°C (Fig. 2 C & D, Braun et al. 2019, n=17 tags).

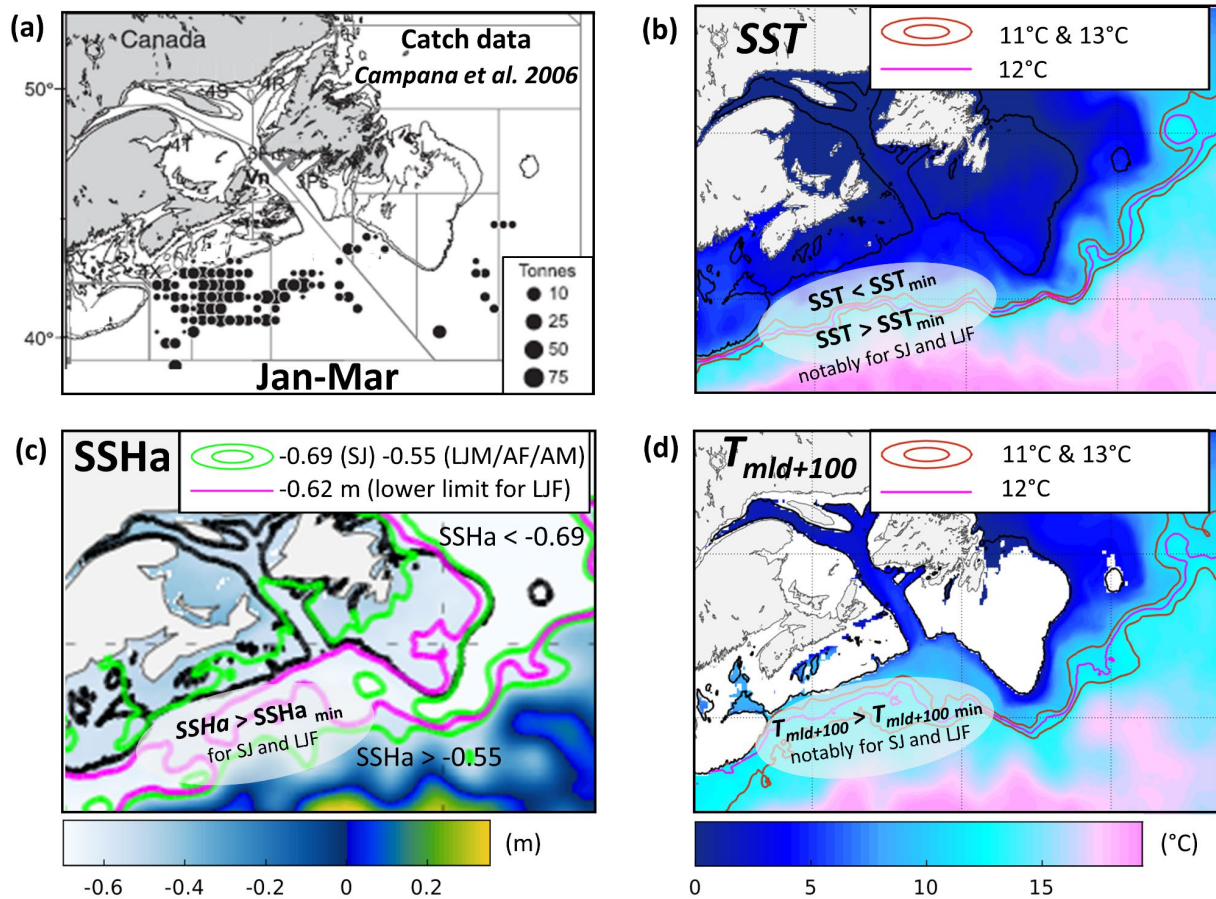


Figure SM.16 Distribution in January-March in the Northwest Atlantic of (a) observer data of blue shark (1986-2004, Campana et al. 2006), and the corresponding distribution of (b) SST, (c) SSHa and (d) $T_{mld+100}$ (temperature 100 m below the mixed layer) (2003-2004, the black line is the 200 m-isodepth contour). The shown isotherms enhance the lower and unsuitable SST levels for blue sharks just off the shelf (below about 11-12°C) while the temperature at depth is warmer and suitable (above about 12°C, notably for small juveniles, SJ, and large juvenile females, LJF). SSHa levels in the area of blue shark presence are mostly suitable for small juveniles (SJ) and large juvenile females (LJF) while mostly unsuitable for large juvenile males (LJM) and adults (AF and AM).

Further qualitative model validation with literature

The figures SM.17-24 below display additional qualitative validation comparing the model predictions with spatial data found in the literature. These independent historic datasets generally agree with the model predictions although the compared years may not always correspond. They further highlight the robustness of the global niche approach, for a widely spread species, to suitably predict habitat in a region where no presence data was used.

Figure SM.17 details the distribution in July-September in the Northwest Atlantic of observer data for blue shark (1986-2004, Campana et al. 2006, upper left panel), the distribution of fork length from recreational fisheries (central left panel), and the corresponding habitat distribution of all classes enhancing the agreement between the LJF catches in the recreational data twice as high than LJM and AM and the respective habitat suitability. Moreover, the SJ class (FL < 125 cm) is underrepresented in the recreational data compared to our observer data (6 to 23-fold higher than the other classes, $n = 2,124$, upper right panel), also in agreement with the corresponding habitat predictions.

Figure SM.18 focuses on the October-December period in the Northwest Atlantic comparing the observer catch data for blue sharks (1986-2004, Campana et al. 2006) and the corresponding habitat distribution of all classes. Note that the individual tracks of blue shark from electronic tagging end in December in the most southern and warmer areas. Both our observer data and habitat suitability in October-December (2003-2018) display substantially lower levels than for the July-September period (Figure SM.17), this contrast with October-December representing the highest catch season in the observer data of Campana et al. (2006). This apparent inconsistency between different observer datasets can likely be associated with seasonally variable fishing effort between 1986-2004 and 2003-2018 periods, the latter period being associated with much higher effort levels.

Figure SM.19 highlights that the area of the maximum catch of blue shark per longline set (purple triangle) may correspond to variable life stages from the habitat modeling results. While the northern part of the triangle may likely correspond to small juveniles and large males, the catches in the western corner may correspond to large juveniles and adult females and the southeast corner to adult females. The seasonal variability (not available in the catch data) may however display large variability of the life stage distribution in both the catch data and habitat prediction. A finer analysis by class and season would be necessary to assess these variable distributions for management.

Figure SM.20 compares the Brazilian longline catch per unit of effort for blue shark (individuals per 1,000 hooks, 2004-2010, Frédou et al. 2015) with large juveniles and adult blue shark habitat in the south Atlantic. The purple boxes highlight some of the maximum CPUE levels in general agreement with the foraging habitat results, notably in the area of 35-45°S for the presented habitat classes but particularly for the large juvenile females (LJF). The 22.5-2.5°W is also characterized by relatively high CPUEs, with lower levels however in the latitude range of 10-35°S in agreement with the avoided SSTs by the females (red isotherm isocontours on the males' maps). The higher catches in the northern part (10°N-10°S, 22.5-12.5°W) are however not suitably captured by the model (except for AF to some extent), but this area presents a particularly high cloud coverage impeding the habitat estimate (see Figure SM.21). The low catch area (15°N-20°S, 47.5-22.5°W) generally agrees with the predictions except in the 0-10°S area for large females.

Figure SM.21 highlights the seasonal changes of foraging habitat along the track of an adult female in the Central Atlantic Ocean (Carvalho et al. 2015) where e.g. the favorable habitat along the shark location in May-June becomes unfavorable in July-September and vice-versa. Apart from the first period (May-June), the habitat predictions are based on the satellite-derived productivity fronts (higher CHL than CHLmin, light blue isocontour), which are mostly missing in the Guinea Current (about 0-5°N, 10°W-10°E) due to cloud coverage in July-August and November-December.

Figure SM.22 compares for January-March in the South Atlantic the observer data of sex ratio and fork length for blue shark (1966-2014, 5° by 5°, Coelho et al. 2018) with the habitat distribution of large juveniles males and females (LJM and LJF) and adult males and females (AM, AF) (2003-2018). While a mix of large males and females is displayed by the catch data in most areas, a particularly low presence of females is shown in the area 30-35°S (purple box) in agreement with the intermediate range of SST identified in the model that is avoided by large females (21.7°C-24°C).

Figure SM.23 shows a similar absence of female catches in the same latitude range and for the same season in the Indian Ocean (January-March, 30-35°S; 20-100°E, purple box). Large female catches tend to be more abundant than large males in the 0-20°S also in agreement with the frequency of favorable foraging habitat of adult females especially. A dominant catch of large juvenile females (and small juveniles to a lower degree, see Figure 5) is both displayed by catch data and model predictions in the area 35-45°S 80-125°E for the period from October to December (purple box, Figure SM.24).

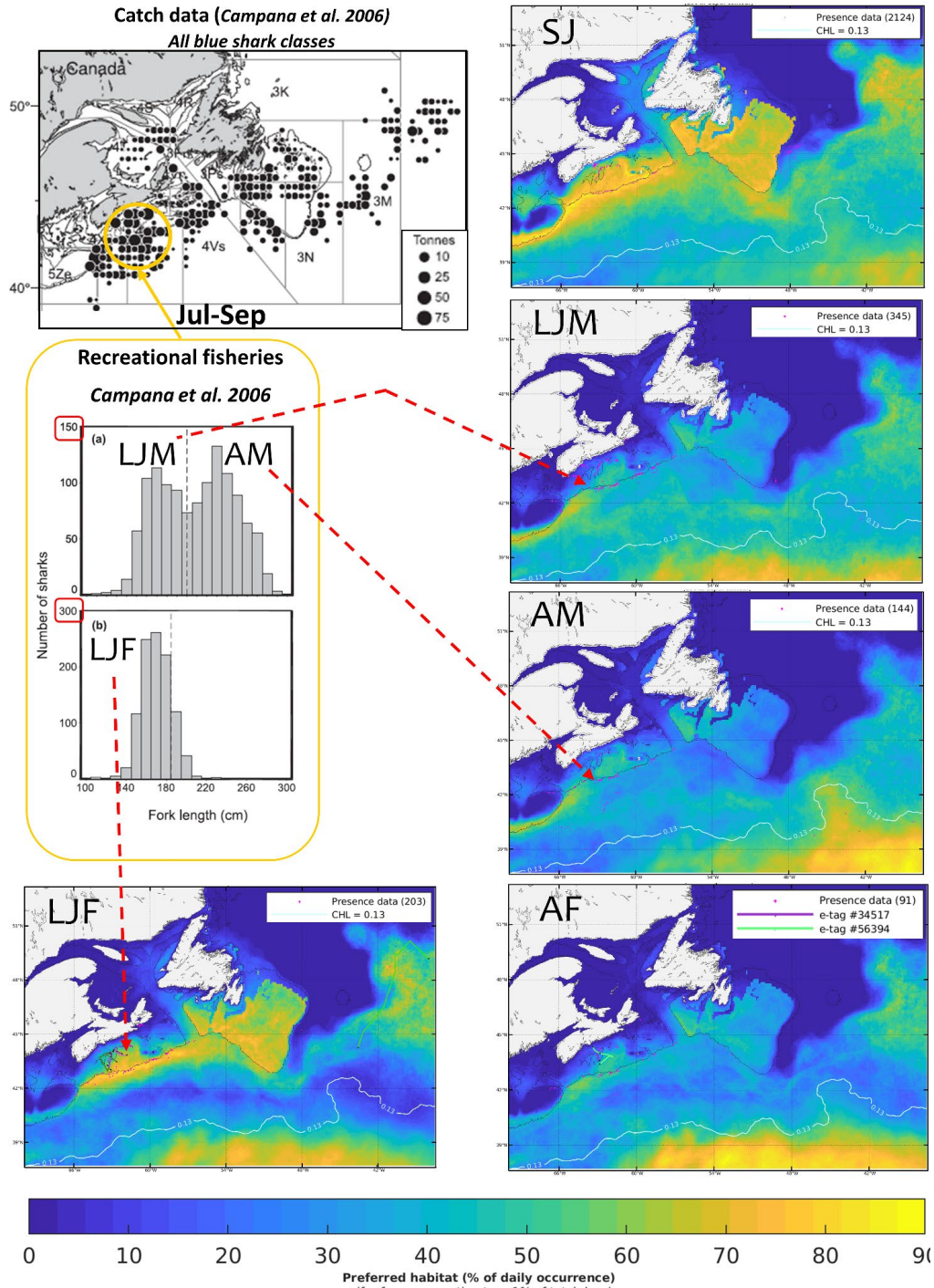


Figure SM.17 Distribution in July-September in the Northwest Atlantic of observer catch data for blue shark (tonnes, 1986-2004, Campana et al. 2006, upper left panel), distribution of fork length from recreational fisheries (central left panel), and corresponding habitat distribution of small juveniles (SJ), large juveniles males and females (LJM and LJF) and adult males and females (AM, AF) (200 m-isodepth contour, black line). The higher *CHL* than lower *CHL_{min}* of 0.13 mg.m⁻³ (light blue isocontour) in the northern part indicates that productivity fronts are used as a foraging proxy in that area.

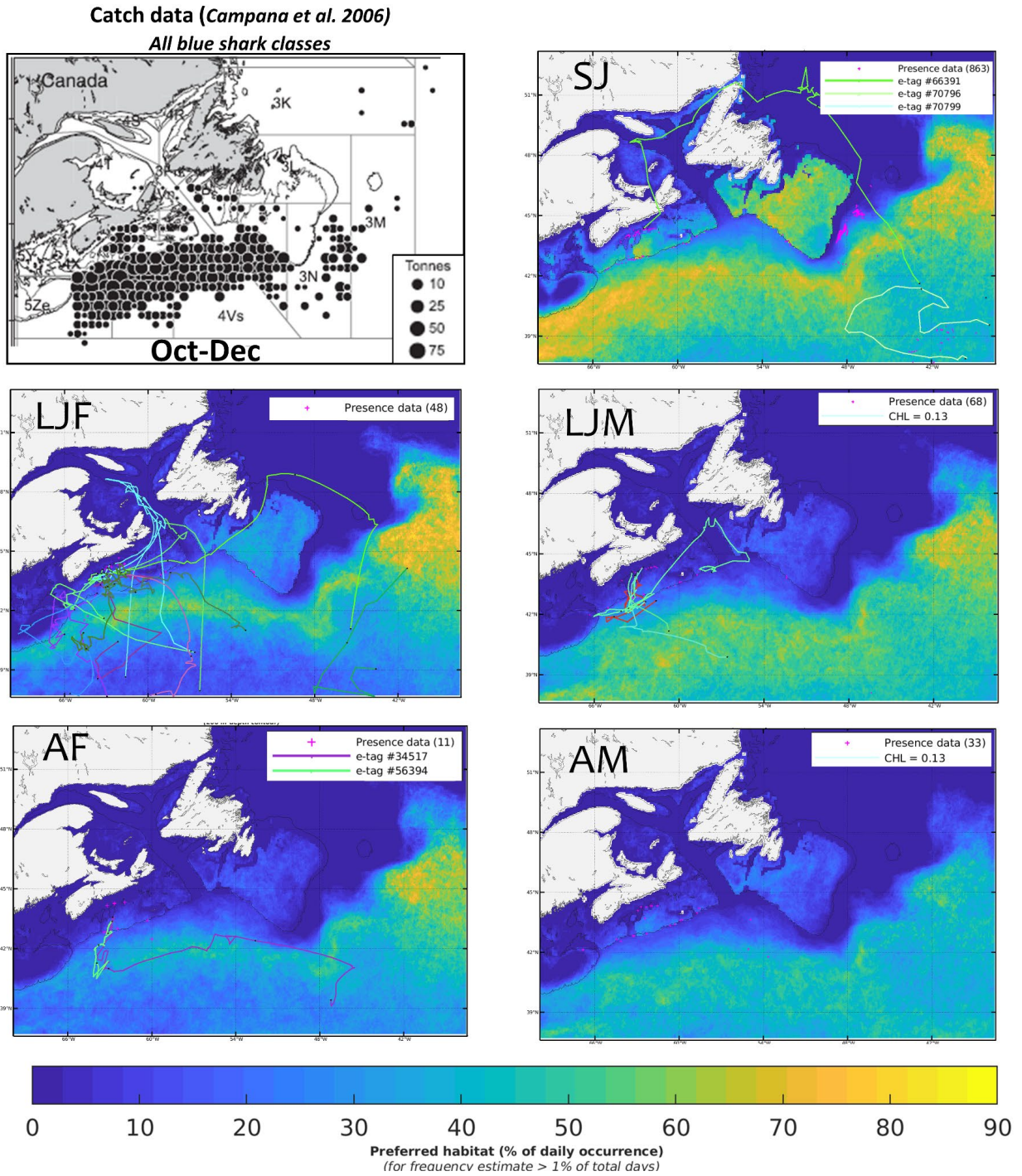


Figure SM.18 Distribution in October-December in the Northwest Atlantic of observer catch data for blue shark (tonnes, 1986-2004, Campana et al. 2006, upper left panel), and corresponding habitat distribution of small juveniles (SJ), large juveniles males and females (LJM and LJF) and adult males and females (AM, AF) (200 m-isodepth contour, black line). The higher CHL than CHL_{min} of $0.13 \text{ mg}\cdot\text{m}^{-3}$ in the entire domain indicates that productivity fronts are used as a foraging proxy in that area.

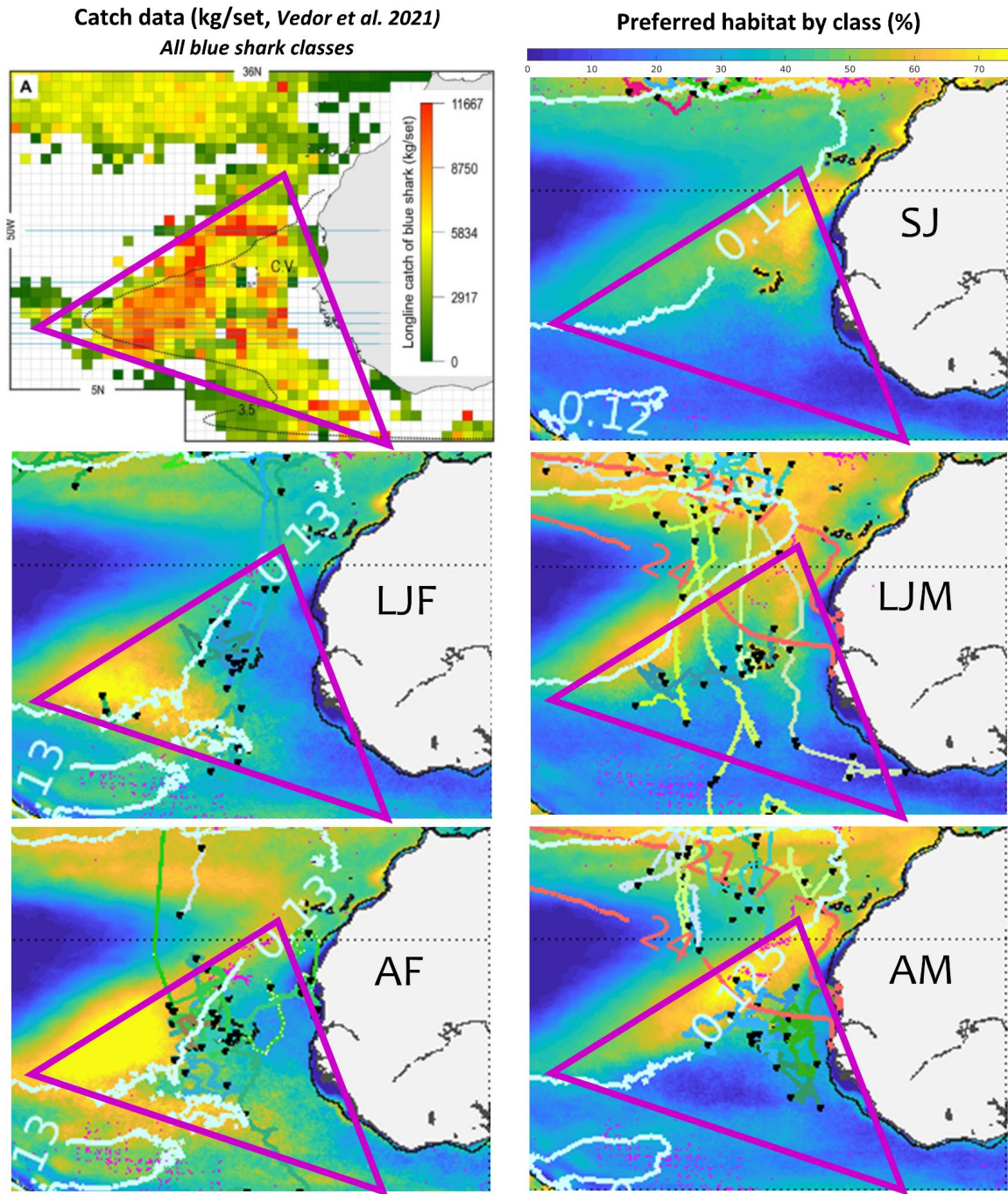


Figure SM.19 Distribution in the eastern Central Atlantic of the Spanish longline catches per unit of effort for blue shark (kg/set, 2013-2018, Vedor et al. 2021, upper left panel), and habitat distribution of small juveniles (SJ), large juveniles males and females (LJM and LJF) and adult males and females (AM, AF) (2003-2018, 200 m-isodepth contour, black line). The lower *CHL* than *CHL_{min}* (light blue isocontour) in the central basin (western area) indicates that estimates of mesopelagic micronekton are used as a foraging proxy in that area, and productivity fronts elsewhere. The purple triangle includes the area of maximum catch per set, which appears to correspond to different size and sex classes from the habitat modeling results.

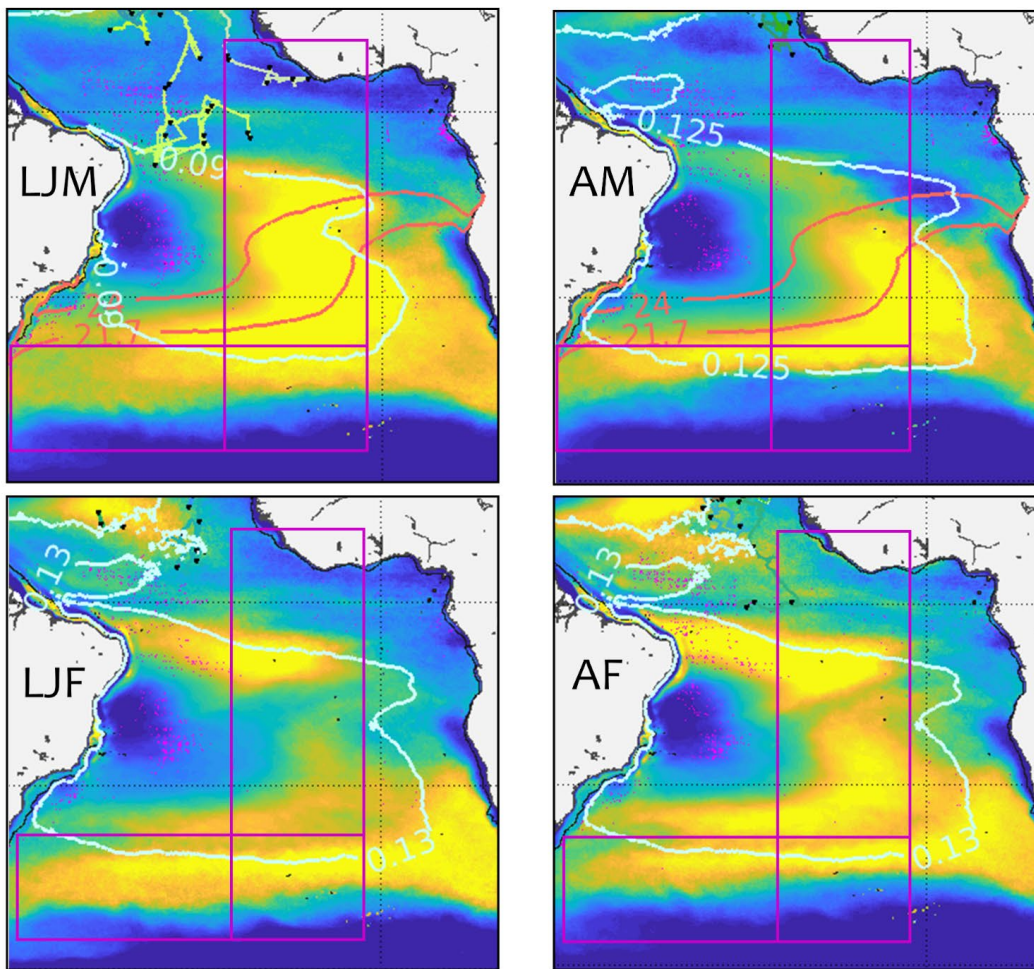
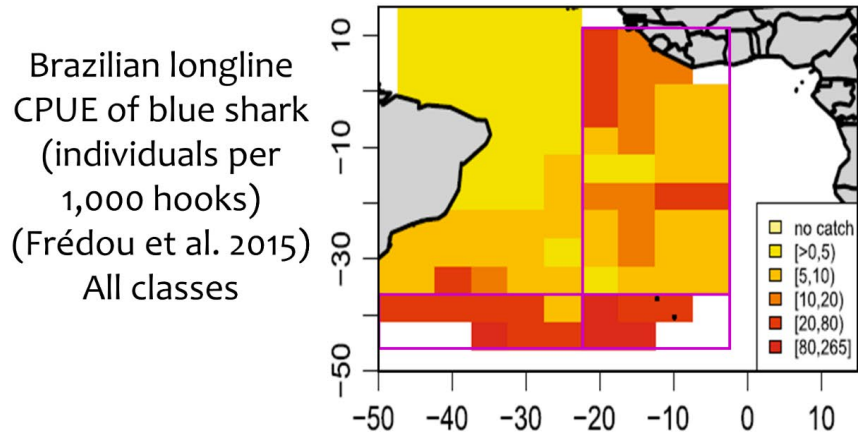


Figure SM.20 Distribution in the South Atlantic of the Brazilian longline catch per unit of effort for blue shark (individuals per 1,000 hooks, 2004-2010, (Frédou et al. 2015), upper panel), and habitat distribution of large juveniles males and females (LJM and LJF) and adult males and females (AM, AF) (2003-2018, 200 m-isodepth contour, black line). The lower *CHL* than *CHL*_{min} (light blue isocontour) in the central basin indicates that estimates of mesopelagic micronekton are used as a foraging proxy in that area, and productivity fronts elsewhere.

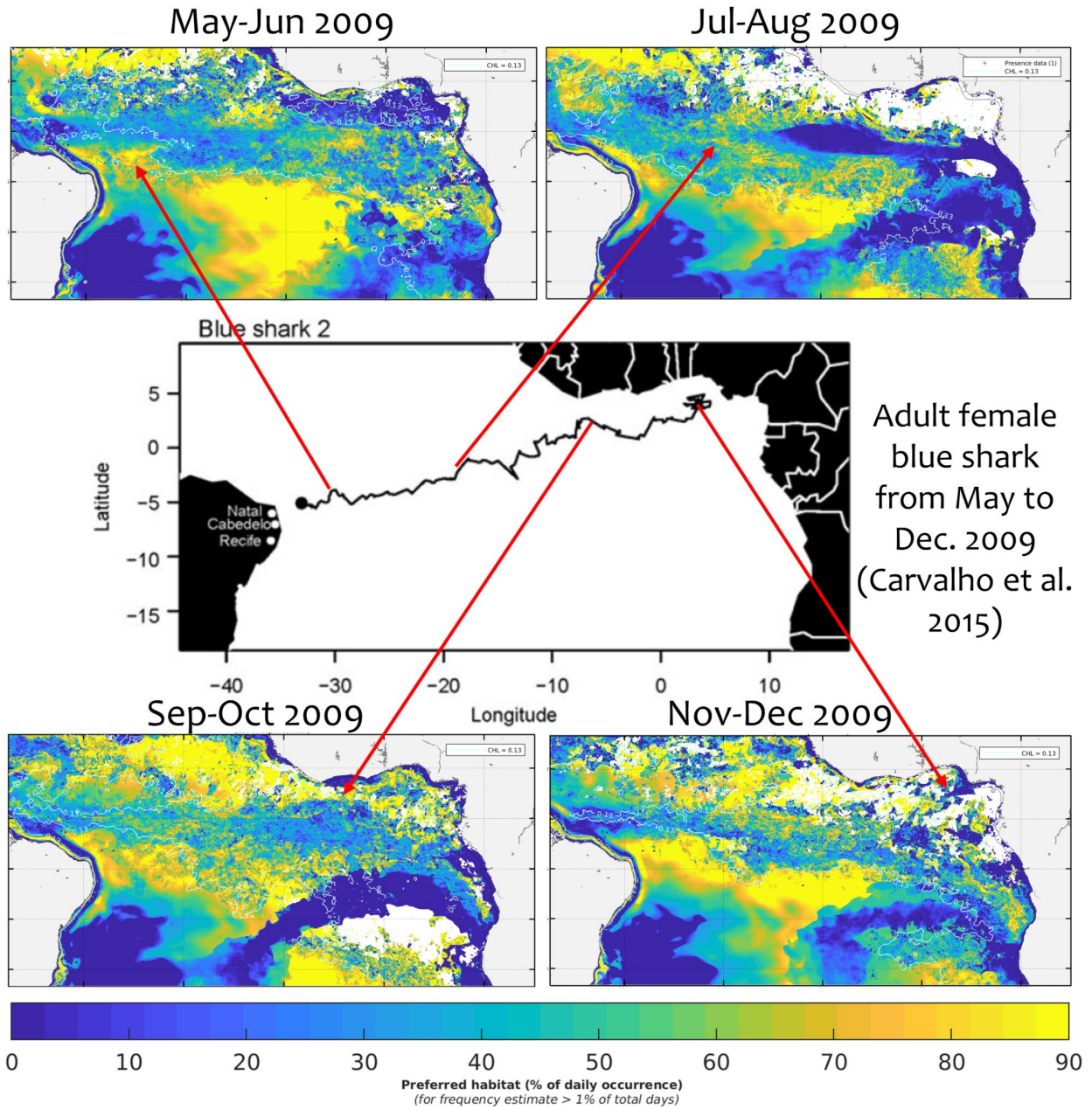


Figure SM.21 Track of an adult female blue shark in the South Atlantic from May to December 2009 (Carvalho et al. 2015, central panel), and corresponding bimonthly habitat predictions.

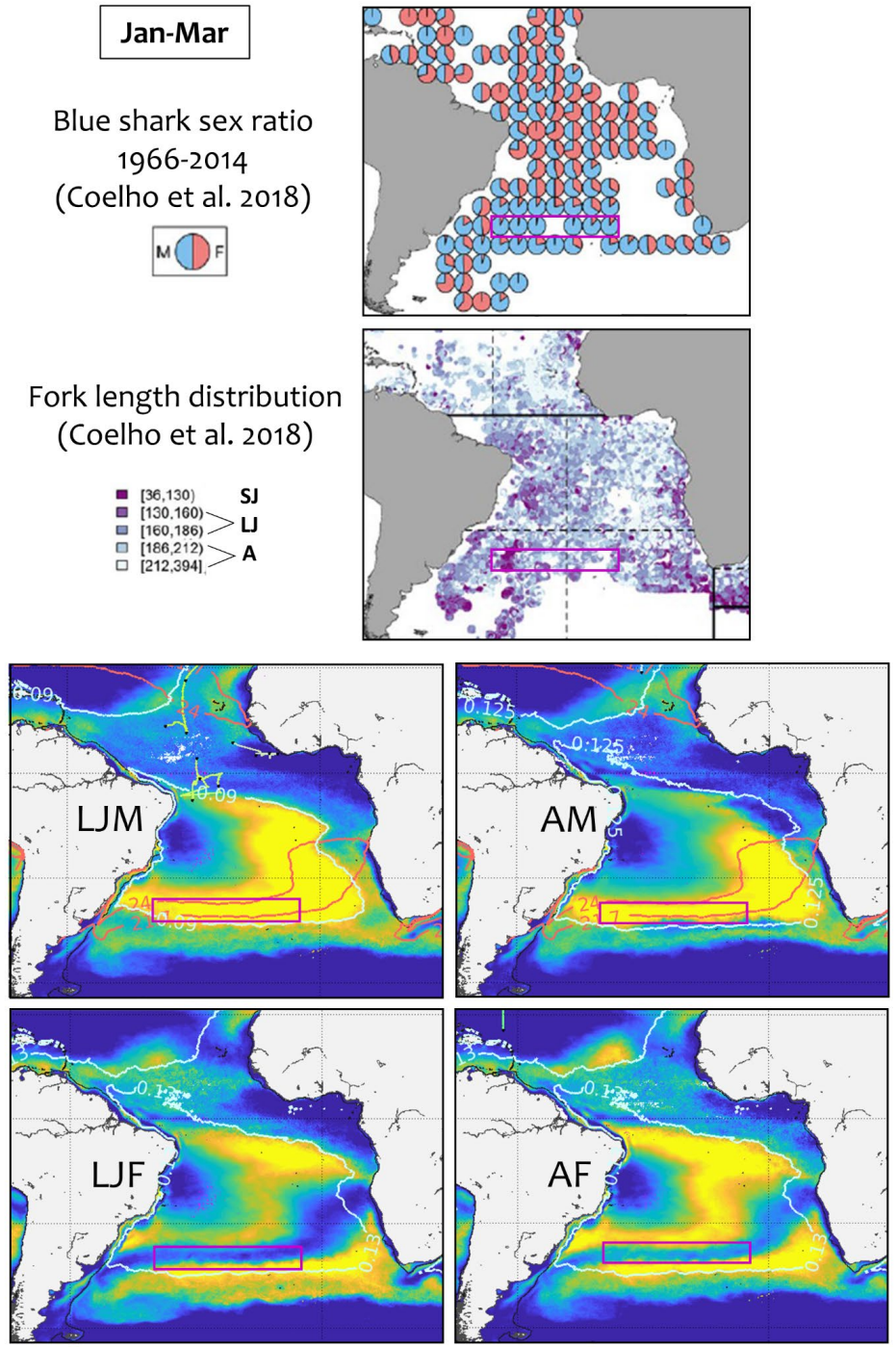


Figure SM.22 Distribution in January-March in the South Atlantic of observer data of sex ratio and fork length for blue shark (1966-2014, Coelho et al. 2018, upper two panels), and habitat distribution of large juveniles males and females (LJM and LJF) and adult males and females (AM, AF) (2003-2018, 200 m-isodepth contour, black line). The lower CHL than CHL_{min} (light blue isocontour) in the central basin indicates that estimates of mesopelagic micronekton are used as a foraging proxy in that area, and productivity fronts elsewhere. Note that male catches in the 30-35°S (purple box) agree to the selected intermediate temperature range avoided by large females.

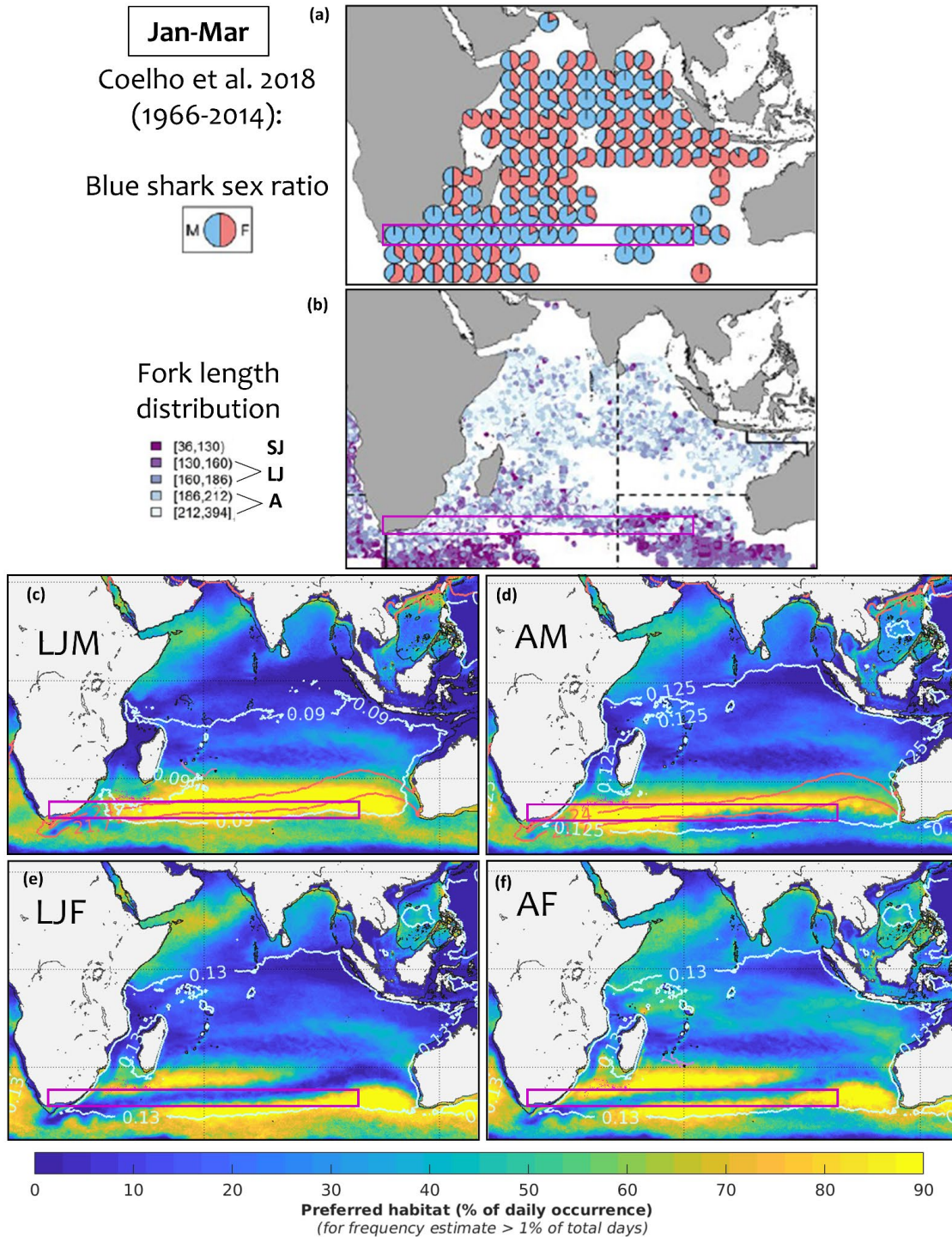


Figure SM.23 Comparison of the blue shark (a) sex ratio and (b) fork length distributions in Jan-Mar in the Indian Ocean on a 5° grid (observer data, 1966-2014, Coelho et al. 2018) with the corresponding foraging habitats of (c) large juvenile males (LJM), (d) adult males (AM), (e) large juvenile females (LJF) and (f) adult females (AF) (2003-2018). The purple box (30-35°S; 20-100°E) shows the presence of large males and the absence of large females in agreement with the habitat results using the intermediate SST levels avoided by females (SST isocontours as red lines).

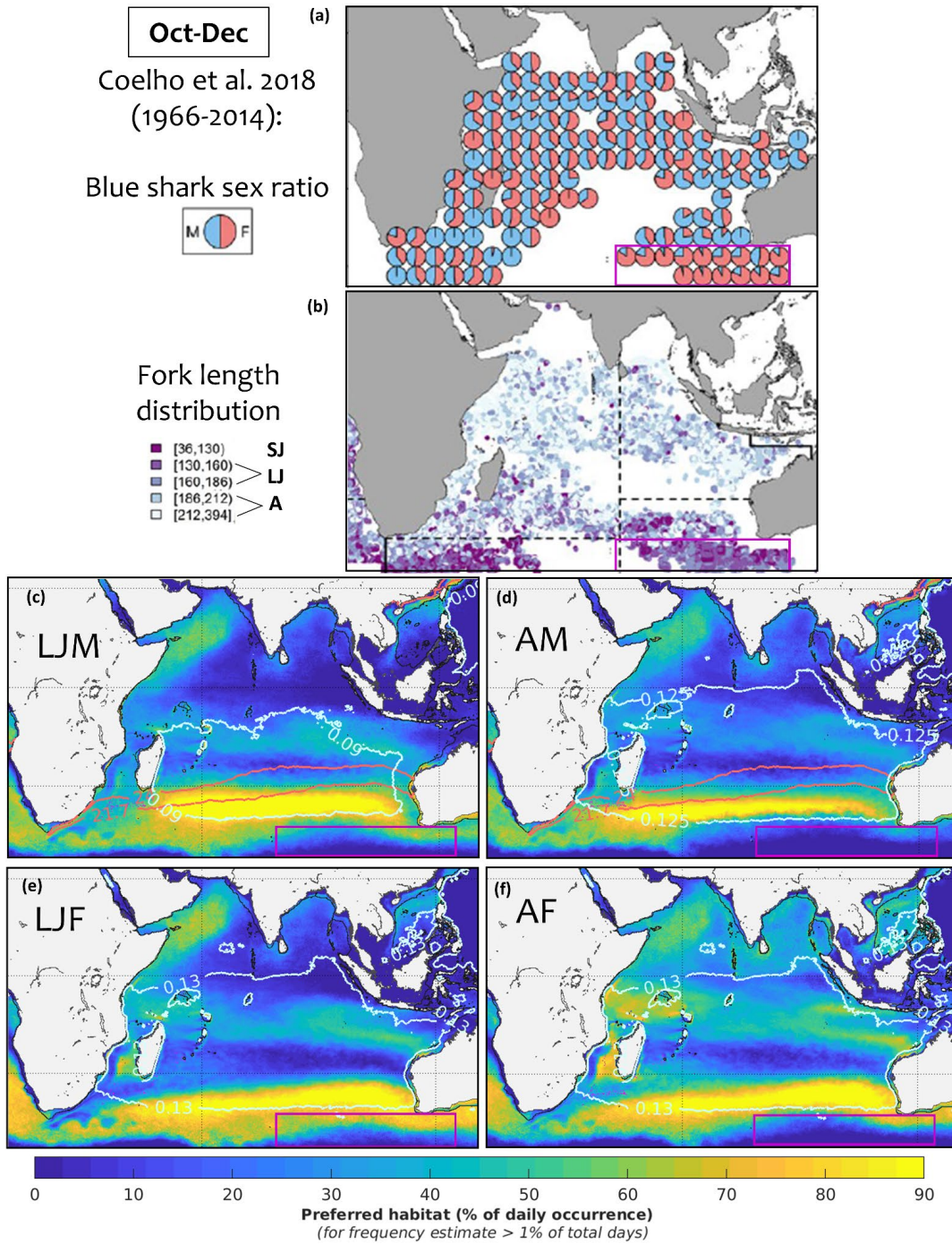


Figure SM.24 Comparison of the blue shark (a) sex ratio and (b) fork length distributions in Oct-Dec in the Indian Ocean on a 5° grid (observer data, 1966-2014, Coelho et al. 2018) with the corresponding foraging habitats of (c) large juvenile males (LJM), (d) adult males (AM), (e) large juvenile females (LJF) and (f) adult females (AF) (2003-2018). The purple box (35-45°S; 80-125°E) shows the predominance of large juvenile females in agreement with the habitat results notably using different lower SST limits as set in the global analysis (SST_{min} of 13.1°C for LJM, 14.8°C for AM, 11.6°C for LJF, 13.3°C for AF; SST_{min} for small juveniles is of 12.3°C - distribution is not shown).

Regional interannual mean and trends of foraging habitat

Interannual mean and absolute trends of foraging habitat expressed in % of habitat occurrence and per year, respectively, were computed at the habitat grid ($1/24^\circ$ resolution) for the period 2003-2018 for each size and sex class (Figures SM.25-26). These regional trend computations provide interesting highlights on the recent displacement of habitat after the current effect of climate change, providing, if substantial, a realistic projection of the habitat modifications in the coming years.

The overall mean absolute trends of habitat for all classes are slightly negative (-0.13 %/yr for SJ and LJF, -0.14 for LJM, -0.12 for AF and AM), however their distribution is highly uneven with substantial negative trends (higher than 15% of habitat occurrence per decade) in large parts of the northern and central Indian Ocean especially for the larger classes and the tropical northern Pacific Ocean. The most important positive trends are displayed in the relatively high latitudes (above 30°) in both hemispheres likely due to the warming of surface waters, except in the observed cooling of the subpolar North Atlantic (Hu and Fedorov 2020). Caution for the interpretation should be taken at the edge of the main gyres where productivity decreases due to ocean warming but where the habitat quality may increase switching foraging proxies from productivity fronts to mesopelagic micronekton (e.g., tropical North Atlantic, eastern North Pacific off California and Mexico).

Overall, the higher losses of habitat over time for blue sharks appear to occur in the equatorial and tropical Indian Ocean and the tropical North Pacific for the juveniles. The major gains of habitat are observed in the Northwest Atlantic and the Mediterranean Sea for the large-size classes, and the temperate South Pacific and Indian Oceans. Interannual contraction and expansion of habitat and the major trends over the last decade should be considered in stock assessment to reduce the uncertainties of the hindcast and forecast estimates.

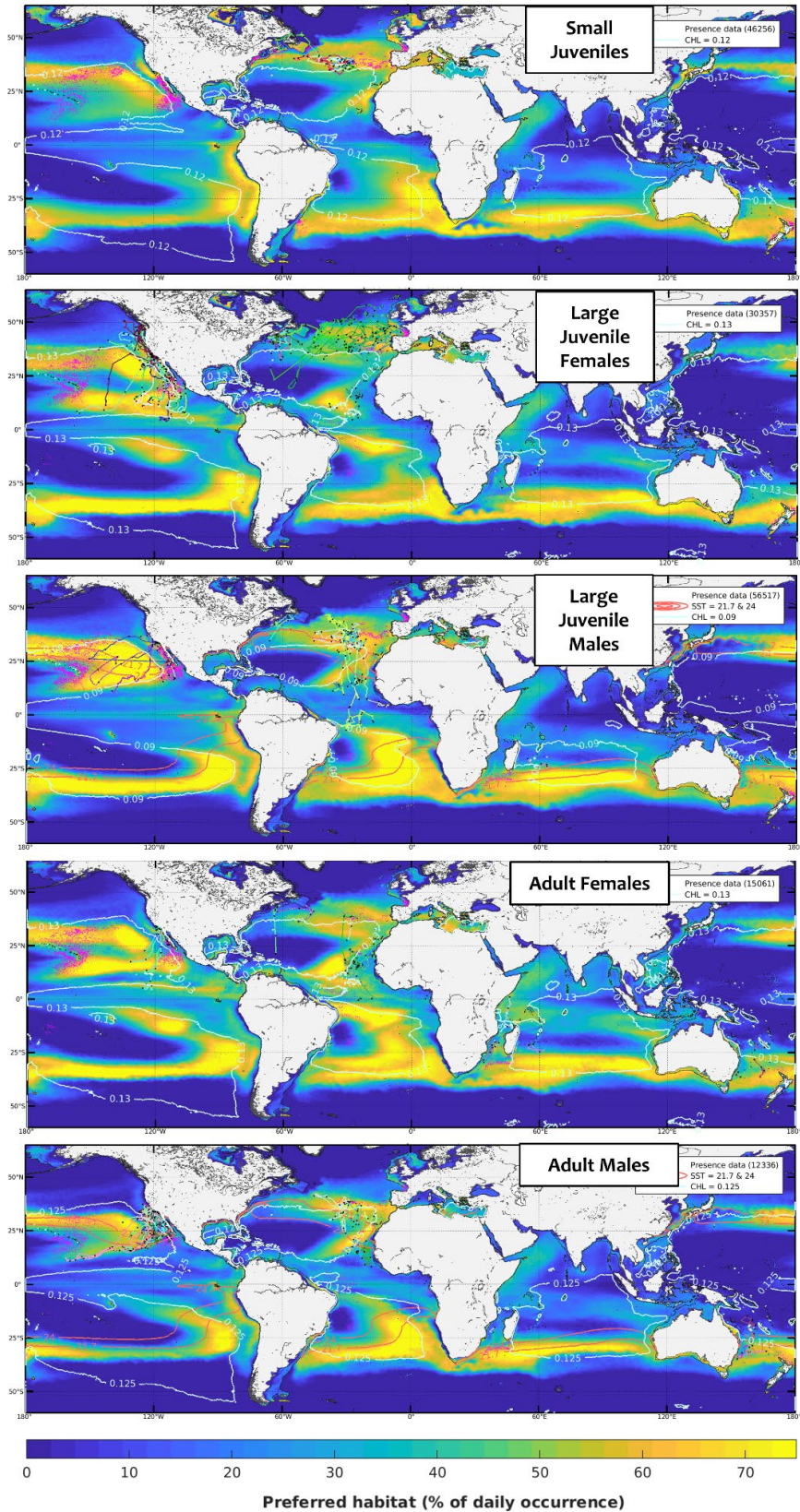


Figure SM.25 Interannual mean of foraging habitat for each blue shark size and sex class (2003-2018, % of habitat occurrence).

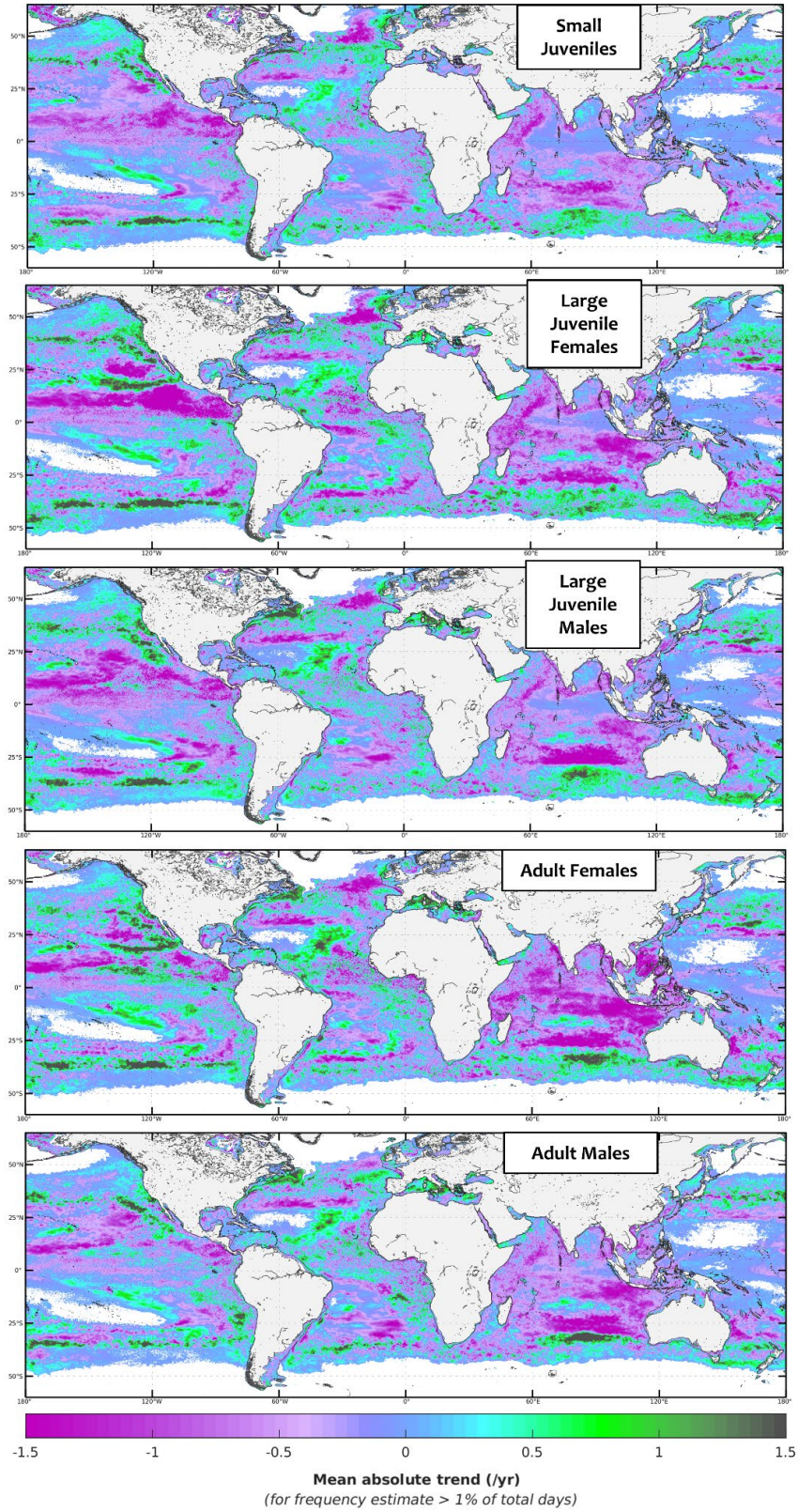


Figure SM.26 Mean absolute trend of foraging habitat for each blue shark size and sex class (2003-2018, %/yr of habitat occurrence). The overall mean habitat trend is -0.13 %/yr for SJ and LJF, -0.14 for LJM, -0.12 for AF and AM.

References

- Berthold, Michael, Christian Borgelt, and Frank Höppner. 2010. *Guide to Intelligent Data Analysis*. Vol. 42. London: Springer, pp. 394.
- Campana, Steven E., Anna Dorey, Mark Fowler, Warren Joyce, Zeliang Wang, Dan Wright, and Igor Yashayaev. 2011. "Migration Pathways, Behavioural Thermoregulation and Overwintering Grounds of Blue Sharks in the Northwest Atlantic." *PloS One* 6 (2): e16854. <https://doi.org/10.1371/journal.pone.0016854>.
- Campana, Steven E., Linda Marks, Warren Joyce, and Nancy E. Kohler. 2006. "Effects of Recreational and Commercial Fishing on Blue Sharks (*Prionace Glauca*) in Atlantic Canada, with Inferences on the North Atlantic Population." *Canadian Journal of Fisheries and Aquatic Sciences* 63 (3): 670–82. <https://doi.org/10.1139/f05-251>.
- Carvalho, Felipe, Robert Ahrens, Debra Murie, Keith Bigelow, Alexandre Aires-Da-Silva, Mark N. Maunder, and Fábio Hazin. 2015. "Using Pop-up Satellite Archival Tags to Inform Selectivity in Fisheries Stock Assessment Models: A Case Study for the Blue Shark in the South Atlantic Ocean." *ICES Journal of Marine Science* 72 (6): 1715–30. <https://doi.org/10.1093/icesjms/fsv026>.
- Coelho, Rui, Jaime Mejuto, Andrés Domingo, Kotaro Yokawa, Kwang-Ming Liu, Enric Cortés, Evgeny V. Romanov, Charlene da Silva, Fábio Hazin, and Freddy Arocha. 2018. "Distribution Patterns and Population Structure of the Blue Shark (*Prionace Glauca*) in the Atlantic and Indian Oceans." *Fish and Fisheries* 19 (1): 90–106. <https://doi.org/10.1111/faf.12238>.
- Costa, Daniel P., Patrick W. Robinson, John PY Arnould, Autumn-Lynn Harrison, Samantha E. Simmons, Jason L. Hassrick, Andrew J. Hoskins, Stephen P. Kirkman, Herman Oosthuizen, and Stella Villegas-Amtmann. 2010. "Accuracy of ARGOS Locations of Pinnipeds At-Sea Estimated Using Fastloc GPS." *PloS One* 5 (1): e8677. <https://doi.org/10.1371/journal.pone.0008677>.
- Druon, Jean-Noël, Antoine Mangin, Pierre Hélaouët, and Andreas Palialexis. 2021. "The Chlorophyll-a Gradient as Primary Earth Observation Index of Marine Ecosystem Feeding Capacity." *Copernicus Marine Service Ocean State Report, Issue 5, Journal of Operational Oceanography*. <https://doi.org/10.1080/1755876X.2021.1946240>.
- Druon, Jean-Noël, Simone Panigada, Léa David, Alexandre Gannier, Pascal Mayol, Antonella Arcangeli, Ana Cañadas, Sophie Laran, Nathalie Di Méglia, and Pauline Gauffier. 2012. "Potential Feeding Habitat of Fin Whales in the Western Mediterranean Sea: An Environmental Niche Model." *Marine Ecology Progress Series* 464: 289–306. <https://doi.org/10.3354/meps09810>.
- Frédou, Flávia Lucena, Mariana Travassos Tolotti, Thierry Frédou, Felipe Carvalho, Humberto Hazin, George Burgess, Rui Coelho, John D. Waters, Paulo Travassos, and Fábio Hissa Vieira Hazin. 2015. "Sharks Caught by the Brazilian Tuna Longline Fleet: An Overview." *Reviews in Fish Biology and Fisheries* 25 (2): 365–77. <https://doi.org/10.1007/s11160-014-9380-8>.
- Hu, Shineng, and Alexey V. Fedorov. 2020. "Indian Ocean Warming as a Driver of the North Atlantic Warming Hole." *Nature Communications* 11 (1): 1–11. <https://doi.org/10.1038/s41467-020-18522-5>.
- Lehodey, Patrick, Anna Conchon, Inna Senina, Réka Domokos, Beatriz Calmettes, Julien Jouanno, Olga Hernandez, and Rudy Kloser. 2015. "Optimization of a Micronekton Model with Acoustic Data." *ICES Journal of Marine Science* 72 (5): 1399–1412. <https://doi.org/10.1093/icesjms/fsu233>.
- Lehodey, Patrick, Raghu Murtugudde, and Inna Senina. 2010. "Bridging the Gap from Ocean Models to Population Dynamics of Large Marine Predators: A Model of Mid-Trophic Functional Groups." *Progress in Oceanography* 84 (1): 69–84. <https://doi.org/10.1016/j.pocean.2009.09.008>.

- MacQueen, James. 1967. "Some Methods for Classification and Analysis of Multivariate Observations." In *Proceedings of the Fifth Berkeley Symposium on Mathematical Statistics and Probability*, 1:14. http://books.google.it/books?hl=it&lr=&id=IC4Ku_7dBFUC&oi=fnd&pg=PA281&dq=Some+methods+for+classification+and+analysis+of+multivariate+observations.&ots=nM_iHXHdsO&sig=srK_0XmiEricJJGxTbCs5toYbTg.
- Pedersen, M. Wever, Toby Alexander Patterson, Uffe Høgsbro Thygesen, and Henrik Madsen. 2011. "Estimating Animal Behavior and Residency from Movement Data." *Oikos* 120 (9): 1281–90. <https://doi.org/10.1111/j.1600-0706.2011.19044.x>.
- Queiroz, Nuno, Nicolas E. Humphries, Gonzalo Mucientes, Neil Hammerschlag, Fernando P. Lima, Kylie L. Scales, Peter I. Miller, Lara L. Sousa, Rui Seabra, and David W. Sims. 2016. "Ocean-Wide Tracking of Pelagic Sharks Reveals Extent of Overlap with Longline Fishing Hotspots." *Proceedings of the National Academy of Sciences* 113 (6): 1582–87. <https://doi.org/10.1073/pnas.1510090113>.
- Vedor, Marisa, Nuno Queiroz, Gonzalo Mucientes, Ana Couto, Ivo da Costa, António Dos Santos, Frederic Vandeperre, et al. 2021. "Climate-Driven Deoxygenation Elevates Fishing Vulnerability for the Ocean's Widest Ranging Shark." *Elife* 10: e62508. <https://doi.org/10.7554/eLife.62508>.